

ASTROCYTIC EXPRESSION OF TDP-43 RESULTS IN NON-CELL AUTONOMOUS
CHANGES

by

DEIDRE LYNN CARTER

A THESIS

Submitted in partial fulfillment of the requirements
For the degree of Master of Science in the
Biological Sciences Graduate Program
of Delaware State University

DOVER, DELAWARE
August 2017

This thesis is approved by the following members of the Final Oral Review Committee:

Dr. Michael Gitcho, Committee Chairperson, Department of Biological Sciences, Delaware State University

Dr. Melissa Harrington, Committee Member, Department of Biological Sciences, Delaware State University

Dr. Hakeem Lawal, Committee Member, Department of Biological Sciences, Delaware State University

Dr. Hacene Boukari, External Committee Member, Department of Physics and Engineering, Delaware State University

DEDICATION

To Mrs. Shonda Poe, Ms. Margie Vela, Dr. Clytrice Watson, Dr. Gulnihal Ozbay, Dr. Lathadevi Chintapenta and Dr. Akwasi Osei for their acts of kindness and kind words during the hard times of this process. Much love and many thank yous to my family and friends: Clara Carter, Charles Carter Sr., Charles Carter Jr., Andrea Carter, Karla Sanchez, Mahlet Mersha, my twins (Myles, Dontray, and Jamie), my BTD cohort, and all of my mentees for picking me up every time I have fallen, failed and every time I was discouraged throughout this process. “For we wrestle not against flesh and blood, but against principalities against powers, against the rulers of the darkness of this world, against spiritual wickedness in high places” – Ephesians 6:12.

ACKNOWLEDGEMENTS

I would like to recognize my PI, Dr. Michael Gitcho and the post-doc on our research team Dr. Stephani Davis for their supervision and combined guidance while I worked on this project. I would also like to recognize my committee: Dr. Hacene Boukari, Dr. Melissa Harrington and Dr. Hakeem Lawal. My work efforts were supported with a fellowship from Philadelphia Louis Stokes Alliance for Minority Participation Bridge to the Doctorate Fellowship. Research reported in this thesis was supported by the Institutional Development Award (IDeA) from the National Institute of Health's National Institute of General Medical Sciences under grant number P20GM103446.

Astrocytic Expression of TDP-43 Results in Non-Cell Autonomous Changes

Deidre Carter

Faculty Advisor: Dr. Michael Gitcho

Abstract

TAR DNA binding protein 43 (TDP-43) is a heterogeneous nuclear ribonucleoprotein that regulates gene expression, RNA stability, and is involved in shuttling back and forth from the nucleus to the cytoplasm. TDP-43 is predominantly localized to the nucleus. Glial Fibrillary Acidic Protein (GFAP) is a major astrocyte marker whose expression increases when astrocytes are activated. We have developed a mouse model that selectively and conditionally expresses a defective nuclear localization signal of TDP-43 (Δ NLS) under control of the astrocytic GFAP promoter to investigate pathological outcomes and non-cell autonomous effects of TDP-43 mis-expression. We hypothesize that GFAP/TDP-43 Δ NLS mice will show non-cell autonomous changes in neurons caused by expression of TDP-43 Δ NLS in astrocytes. In order to characterize this model of astrocyte expression, an exon array was used to examine global changes in RNA expression/splicing in the spinal cord of two-month old mice. In addition, immunohistochemistry in both two-month old and six-month-old mice reveal age-dependent changes in myelin basic protein. At two months of age GFAP/TDP-43 Δ NLS mice display functional changes in memory, which may be associated with the changes in myelination observed. Primary cortical neuron/astrocyte co-cultures expressing TDP-43 Δ NLS exclusively in astrocytes show a significant

decrease in neurons (as shown by β III-tubulin immunoreactivity) compared with littermate controls. These data suggest that astrocytic expression of TDP-43 Δ NLS alters neuronal function both *in vitro* and *in vivo*. This study may provide insight and a better understanding of how astrocytic accumulation/aggregation of TDP-43 contributes to neurodegeneration.

TABLE OF CONTENTS

	Page
List of Tables	vii
List of Figures	viii
List of Abbreviations	ix
CHAPTER 1: INTRODUCTION	1
CHAPTER 2: LITERATURE REVIEW	3
2.1 <i>Heterogeneity of Astrocytes in the CNS</i>	6
2.2 <i>Astrocytes involvement in memory changes and neurodegeneration</i>	8
CHAPTER 3: MATERIALS AND METHODS	11
3.1 <i>Animals</i>	11
3.2 <i>Primary Cortical Neuron Cultures</i>	11
3.3 <i>Radial Arm Maze</i>	13
3.4 <i>Y maze</i>	13
3.5 <i>Immunohistochemistry</i>	14
3.6 <i>RNA Extraction</i>	15
3.7 <i>Data Analysis</i>	16
CHAPTER 4: RESULTS	17
4.1 <i>Non-cell autonomous changes are observed in vitro</i>	17
4.2 <i>Astrocyte specific expression of TDP-43ΔNLS induces memory deficits</i>	20
4.3 <i>TDP-43ΔNLS induces abnormal expression in brain and spinal cord</i>	23
4.4 <i>GFAP/TDP-43ΔNLS mice show age dependent change in Myelin Basic Protein Expression</i>	28
4.5 <i>Exploration of gene expression and splicing via exon array</i>	29
CHAPTER 5: DISCUSSION	31
References.....	37
Appendix A: Schematic of Apparatus used for memory studies	45
Appendix B: TDP-43 Alternative Gene splicing in GFAP/TDP-43 Δ NLS model.....	46

LIST OF TABLES

	Page
<i>Table 1. Overview of TDP-43 splicing in GFAP/TDP-43ΔNLS model</i>	29

LIST OF FIGURES

	Page
<i>Figure 1.</i> hTDP-43 localizes to the cytoplasm of GFAP/TDP-43ΔNLS astrocytes.....	18
<i>Figure 2.</i> TDP-43 is present in nucleus and cytoplasm <i>in vitro</i>	19
<i>Figure 3.</i> Neuron structure changes are observed in GFAP/TDP-43ΔNLS primary cultures	20
<i>Figure 4.</i> Spatial memory deficits are observed in 2-month old GFAP/TDP-43ΔNLS mice	21
<i>Figure 5.</i> Exploratory behavior and working memory changes are observed in 2-month old GFAP/TDP-43ΔNLS mice.....	22
<i>Figure 6</i> Nissl Stain reveals changes in motor neuron structure in GFAP/TDP-43ΔNLS mice	24
<i>Figure 7.</i> TDP-43ΔNLS exposes heterogeneity of astrocytes in dentate gyrus	25
<i>Figure 8.</i> TDP-43ΔNLS induces increase of TDP-43 correlated with age in dentate gyrus	26
<i>Figure 9.</i> Myelin basic protein expression pattern is altered in dentate gyrus due to astrocytic expression of TDP-43ΔNLS.....	27
<i>Figure 10.</i> Grey matter of spinal cord shows changes in myelin basic protein expression	28

LIST OF ABBREVIATIONS

CNS.....	Central Nervous System
GFAP	Glial Fibrillary Acidic Protein
hGFAP	human specific Glial Fibrillary Acidic Protein
hTDP-43.....	human specific TAR DNA Binding Protein 43kDa
kDA.....	Kilodaltons
MBP	Myelin Basic Protein
NLS.....	Nuclear Localization Signal
PFA	paraformaldehyde
TDP-43 Δ NLS.....	TAR DNA Binding Protein 43kDa with defective NLS
TDP-43.....	TAR DNA Binding Protein 43kDa
WT	Wild-Type

CHAPTER 1: INTRODUCTION

TAR DNA binding protein 43 (TDP-43) is a heterogeneous nuclear ribonucleoprotein. It is a multifunctional protein that is known to aid in RNA stability and regulation of gene expression via splicing. TDP-43 has shuttling properties known as nuclear localization signals (NLS) and nuclear export signals (NES) which is enabled by bipartite sequence in the TARDBP gene (Y. M. Ayala et al., 2008; Winton et al., 2008). In this study, we focused on the inability of TDP-43 to localize to the nucleus by introducing a missense mutation among the known NLS bipartite sequence (NLS1 K82RK84 and NLS2 K95KR98) (Y. M. Ayala et al., 2008). The missense mutation introduces alanine into the sequence and creates a defective nuclear localization signal (Δ NLS) inhibiting TDP-43 from entering the nucleus therefore it localizes to the cytoplasm. TDP-43 Δ NLS. Pathological TDP-43 is known to be hyperphosphorylated, mislocalized and forms cytoplasmic stress granules that lead to pathological aggregates (Cohen, Lee, & Trojanowski, 2012). Toxic aggregates contribute to TDP-43-mediated gain of function pathology. TDP-43 is the major pathological protein in frontotemporal lobar degeneration with ubiquitin inclusions (FTLD-U) and amyotrophic lateral sclerosis (ALS) (Gendron, T.F.; Josephs, K.A; Petrucelli, 2011).

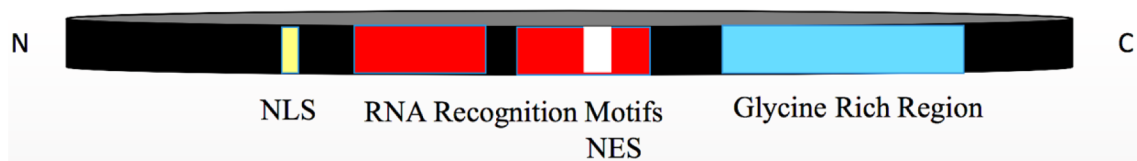
Neurodegeneration as well as neurodevelopment is caused by more than just death of neurons. It is understood that glia such as astrocytes play a role in neuro-diseases and mechanisms (Ben Haim, Carrillo-de Sauvage, Ceyzeriat, & Escartin, 2015). Astrocytes and their multi-faceted involvement in the nervous system are a popular focus for neuroglia, especially exploring heterogeneity and the roles of astrocyte subtypes. Astrocytes are found in both white

matter and grey matter and their roles within tissue varies from myelin development and repair to supporting neurons in metabolism and neurotransmitter release and synapse formation (Sofroniew & Vinters, 2010). Astrocytes are key players in the nervous system whose role has been under-studied in neurodegenerative diseases.

CHAPTER 2: LITERATURE REVIEW

As the quality of living progressively improves over time, people are living longer lives. Therefore, neurodegeneration is becoming a focus in neuroscience because the human body is affected by age dependent changes. One protein that has been identified as a key player in neurodegenerative pathology is TDP-43 (Cykowski et al., 2016; Gendron, T.F.; Josephs, K.A.; Petrucelli, 2011; Huang, 2015; Yang et al., 2014). Trans-active response DNA-binding protein (TDP-43) is a heterogeneous nuclear ribonucleoprotein that is highly conserved and expressed in many tissues. TDP-43 is both a DNA and RNA binding protein which allows regulation of gene expression through transcription, mRNA stability and alternative splicing (Cohen et al., 2012; Tollervey, Curk, Rogelj, Briese, & Cereda, 2011; Winton et al., 2008). It consists of two RNA recognition motifs and a glycine rich C-terminus domain (Youhna M Ayala et al., 2011; Buratti, Baralle, Buratti, & Baralle, 2017; Tollervey et al., 2011).

TDP-43 also contains a nuclear localization signal (NLS) which allows shuttling of the protein between the nucleus and the cytoplasm. Two important components of the structure of TDP-43 is the nuclear localization signal (NLS) and nuclear export signal (NES) which aids in TDP-43 function and pathogenesis (Wobst, Delsing, Brandon, & Moss, 2017). A defective NLS (denoted as Δ NLS) results in aggregation of TDP-43 in the cytoplasm (Winton et al., 2008; Yang et al., 2014). This cytoplasmic aggregation is toxic for the cells such as neurons, motor neurons and even astrocytes (Heaven et al., 2016; Yu-chih Liu, Chiang, & Tsai, 2013; Perng et al., 2006; Yang et al., 2014).



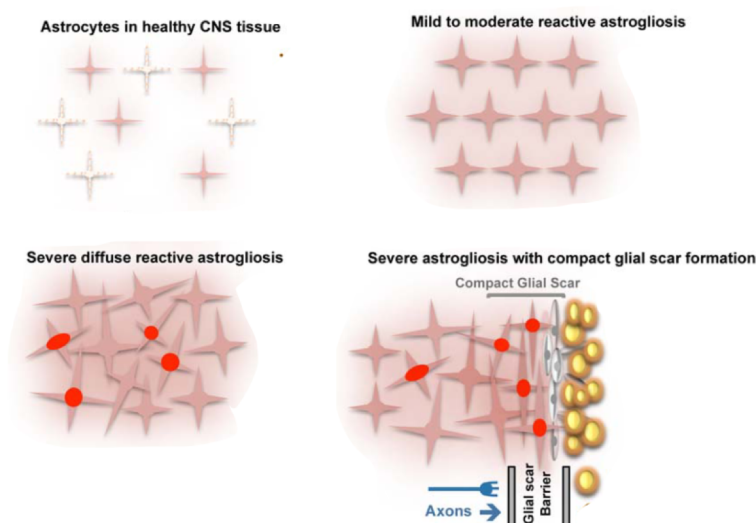
Schematic for TARDBP Gene

TDP-43 gene (black) is 414 amino acids and 43kDa. It contains a nuclear localization signal, NLS (yellow) nuclear export signal, NES (white), two RNA recognition motifs (red) and a glycine rich region (blue) near the C-terminus. Schematic modified from (Y. M. Ayala et al., 2008; Cohen et al., 2012; Winton et al., 2008)

TDP-43 is known to bind mRNA through (GU)₆ rich repeats in RNA (Y. M. Ayala et al., 2008). This helps TDP-43 as it self regulates through a negative feedback loop at the level of transcription (Youhna M Ayala et al., 2011). Ayala et al used qPCR to determine that TDP-43 will bind to itself in the 3' UTR to activate this feedback mechanism. TDP-43 pathologies such as ΔNLS, accumulation and aggregation as well as TDP-43 mutations in the gene are causative factors of many ALS and FTD cases (reviewed in Cohen et al., 2012). Although TDP-43 and neurons play a major role in neurodegeneration, researchers are shifting the focus to observe effects that neurodegeneration has on glia and vice versa (De Keyser, Mostert, & Koch, 2008).

Understanding the role of astrocytes is a popular and essential trend in neuroscience. In 1893, the term astrocyte was coined by Michael von Lenhossek, to describe the morphology of a specific neuroglia whose morphology resembled stars (reviewed in Oberheim, Goldman, & Nedergaard, 2012). Astrocytes have since been understood as a heterogeneous population of glial cells. Astrocytes function as aids in development, regulation of blood flow, formation of synapse via initiation, maturation and termination of synapses, homeostasis by regulation fluid, ions, pH and neurotransmitters through transporters, exchangers and aquaporins and serve as markers for insult to the central nervous system (reviewed in Domingues, Portugal, Socodato, &

Relvas, 2016; Sofroniew & Vinters, 2010). When damaged or diseased tissue is present in the central nervous system, astrocytes are presented in a pathological form known as reactive astrogliosis (Bushong, Martone, & Ellisman, 2004; Wilhelmsson, 2004). There are three forms of reactive astrogliosis: mild to moderate, severe diffuse and severe with compact glial scar formation. In mild to moderate reactive astrogliosis, there is a presence of hypertrophic astrocytes, very slight astrocyte proliferation, functional variability and an up-regulation of an astrocyte marker, glial fibrillary acidic protein (GFAP).



Schematic for Reactive Astrogliosis in Central Nervous System tissue

Illustrations show astrocytes in four situations that are known to occur in the central nervous system.

Astrocytes in healthy CNS tissue are uniformly distributed with domains that do not overlap. Color and pattern of astrocytes are symbolic of GFAP levels. GFAP levels fluctuate and may not be heavily expressed in all astrocytes. Astrocyte domains progressively become disturbed in mild to moderate reactive astrogliosis

As reactive astrogliosis progresses in severe diffuse reactive gliosis, astrocytes begin to proliferate (symbolized with red nuclei). In the most severe form of astrogliosis, a compact glial scar is formed by non-CNS cells such as inflammatory cells, and infectious agents rushing to the site of injury to contribute with glia cells in scar formation. Images adapted from (Sofroniew & Vinters, 2010)

Severe diffuse reactive astrogliosis displays hypertrophic astrocytes, astrocyte proliferation, up-regulation of GFAP, disruption of established astrocyte domains, and may result in a new pattern of neural tissue formation due to responses to neurodegeneration. Severe reactive gliosis with glial scar formation will present itself similar to severe reactive astrogliosis and will attract

inflammatory cells and astrocytes will border damaged tissue. Astrocytes will continue to proliferate and overlap to form a glial scar at the site of the damaged tissue or neuronal insult (reviewed in Sofroniew & Vinters, 2010). A glial scar will prevent any further damage from occurring at this insult site.

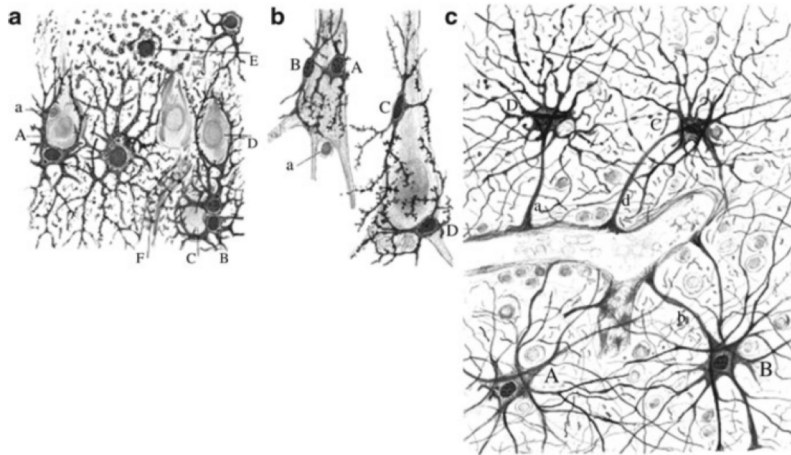
Previously mentioned, GFAP is an intermediate filament protein that is commonly considered to be a primary astrocyte marker (Wilhelmsson, 2004). Recent research suggests that not all astrocytes in the central nervous system express GFAP because there is a diverse population of astrocyte subtypes and GFAP is turned on later in development (Emsley & Macklis, 2007; Molofsky et al., 2012; A. Serio et al., 2013; Vasile, Dossi, & Rouach, 2017). Other astrocyte markers such as S100 β , Vimentin, GLAST, and CD44 marker astrocytes as well as progenitors but there are many caveats to these markers. Some of these caveats include co-expression in neurons, oligodendrocyte progenitors and oligodendrocytes, expression in radial glia and researcher's inability to accurately determine the cell fate and lack of complete characterization (reviewed in Molofsky et al., 2012). Astrocytes are no longer considered one cell type because they are a complex family of glia.

2.1 Heterogeneity of Astrocytes in the CNS

Scientists such as Virchow, Deiters, Golgi, Ramon y Cajal, Lenhossek, have contributed tremendously to the knowledge of astrocytes (reviewed in Chvátal et al., 2008; Oberheim et al., 2012). Virchow initially published and popularized the work of another researcher and concluded that all living things come from other living things. This translated to the consideration of connective tissue of the brain being composed of neuroglia and other cellular elements. In 1865, Otto Deiters used chromic acid carmine red to stain and study neurons and glia. By using advances in microscopy, Deiters was able to publish the first picture of an

astrocyte (reviewed in Chandrasekaran, Avci, Leist, Kobolák, & Dinnyés, 2016). Later, Golgi visualized astrocytes through a silver impregnation technique commonly known as the Golgi stain and contributed to the knowledge of astrocytes with the concept that astrocytes are like glue in the central nervous system (Bushong et al., 2004). In the late nineteenth century, Michael von Lenhossek coined the term astrocyte (Stahnisch & Bulloch, 2011). Ramon y Cajal later drew different subtypes of astrocytes and allowed the appreciation and realization for the importance astrocytes in the central nervous system (Oberheim et al., 2012). Protoplasmic and fibrous astrocytes were identified and appreciated by using the Golgi stain. Protoplasmic astrocytes are found in grey matter, whereas fibrous astrocytes are found in white matter. Protoplasmic astrocytes contain a complex distribution of branching processes attached to the cell body of the astrocyte. Fibrous astrocytes are longitudinal and contain less processes and branching (Emsley & Macklis, 2007). Researchers can further classify astrocyte type by morphology and location.

Although astrocyte types have different morphology and distinct functions, they are known to ubiquitously express GFAP in varied levels. Ayala *et al* grew protoplasmic astrocytes *in vitro* as co-cultures with neural stem cells. They accurately labeled protoplasmic astrocytes with GFAP. Magavi et al took a different approach to explore protoplasmic astrocytes by CRE/LOX system in mice to express green fluorescent protein, (GFP) in the neocortex. Protoplasmic astrocytes *in vivo* were GFP⁺ which helped identify these astrocytes (Magavi, Friedmann, Banks, Stolfi, & Lois, 2012).



Drawings by Ramon y Cajal of astrocyte morphologies observed under microscope by gold chloride staining method

These drawings are representative of astrocytes observed in the pyramidal layer of the human hippocampus. (a) The pyramidal layer of the hippocampus (labeled “D”), and astrocytes (labeled “A” and “B”). (b) Heterogeneity of astrocytes are denoted by “A”, “B”, “C”, “D”. Astrocytes are surrounding neuronal cell bodies in the pyramidal layer. “B” shows an astrocyte with longitudinal properties and minimal branched processes. “D” shows an astrocyte with many complex branched processes. (c) Astrocytes were observed surrounding a blood vessel. Images adapted from (Oberheim et al., 2012)

2.2 Astrocytes involvement in memory changes and neurodegeneration

With astrocytes and subtypes of astrocytes becoming an essential focus in neuroscience, it is becoming more evident that astrocytes play a role in development disorders such as autism and Alexander’s Disease. Astrocytes also play a role in degeneration seen in Alzheimer’s disease, schizophrenia, ALS and leukodystrophies like Alexander’s Disease (Ben Haim et al., 2015; De Keyser et al., 2008; Perng et al., 2006). Mechanisms such as metabolic support, neurogenesis (or the lack thereof), and gliotransmitters contribute to memory. Memory is modulated through neuron-astrocyte interaction and cross-talk. Specifically, protoplasmic astrocytes promote and support differentiation from neural stem cells to neurons (Yuan Liu, Wang, Long, Zeng, & Wu, 2012). Liu *et al* used neural stem cells *in vitro* co-cultured with protoplasmic astrocytes to promote and enhance neuron differentiation and growth. Although heterogeneity of astrocytes and their roles in the central nervous system are under-studied,

protoplasmic astrocytes may be essential for promotion of neurogenesis and the formation and retention of memory. Adult neurogenesis contributes to memory via new neurons in the dentate gyrus (Choi et al., 2016). Altered expression of astrocytes and abnormalities in astrocytes impair neurogenesis, therefore affecting memory (Adamsky & Goshen, 2017; Orellana, Retamal, Moraga-Amaro, & Stehberg, 2016). Long term potentiation is essential in memory formation (Henneberger, Papouin, Oliet, & Rusakov, 2010; Zhang, Zhang, & Chen, 2009). Newman *et al* studied the role of astrocytes in memory by injecting glucose into the hippocampus of rats because glucose is a modulator of memory and enhances memory. Astrocytes uptake the glucose that was injected and stored it as glycogen (verified through immunolabeling). They tested the rats in a spatial working memory test and their results showed that glucose levels decreased while lactate levels increased which was a result of glycogenolysis in astrocytes (Newman, Korol, & Gold, 2011). Models to study the role that astrocytes play in memory use optogenetics, chemogenetics, and electrophysiology to understand the mechanisms of memory, but rodent models and even *C.elegans* are sufficient to study the behavior and memory (Adamsky & Goshen, 2017; Foley et al., 2008; Tsao et al., 2012).

Neurodevelopment and neurodegeneration can be studied by using many models, but a common and popular model are rodent models. Alexander's disease is an ideal model to study neurodevelopment and neurodegeneration from a neuroglia viewpoint because it is a primary astrogliaopathy. Primary astrogliaopathies are disorders or diseases that occur from primary pathogenesis occurring in astrocytes. In Alexander's disease, pathology is caused by mutations in the GFAP gene and overexpression of GFAP. GFAP becomes insoluble and forms aggregates with alpha-beta crystalline, TDP-43 and HSP-27 (Heaven et al., 2016; Olabarria, Putilina, Riemer, & Goldman, 2015). Demyelination is a pathological hallmark of Alexander's disease.

Astrocytic abnormalities are a suspect in leukodystrophies as well as neurodevelopment and neurodegeneration (Heaven et al., 2016; Olabarria et al., 2015; Walker et al., 2014).

GFAP and TDP-43 together are pathogenically present in neurodegeneration as a form of reactive astrogliosis, accumulation or aggregation (A. Serio et al., 2013; Tsao et al., 2012). Estes *et al* used *Drosophila* as a model to study amyotrophic lateral sclerosis (ALS). This model expressed mutations known to cause ALS and downstream effects were analyzed by immunofluorescence, live imaging and western blotting. By expressing ALS causative mutations, this research team found that mutant TDP-43 and TDP-43 overexpression in the cytoplasm of glia resulted in TDP-43 punctate staining. Overexpression of mutant TDP-43 did not affect the shape of neurons but *in vitro* TDP-43 was observed in motor neurons. TDP-43 was only found in motor neurons *in vitro* and not *in vivo* and was present as punctate staining (Estes et al., 2013).

There has been gaps in many studies regarding the involvement of TDP-43 Δ NLS and the role that TDP-43 plays in astrocytes. Our study will investigate how cytoplasmic expression of TDP-43 Δ NLS in astrocytes affects memory and degeneration and *in vitro* and *in vivo* dynamics for cells.

CHAPTER 3: MATERIALS AND METHODS

3.1 Animals

All animal protocols were conducted in accordance with the United States Public Health Service Guide for the Care and Use of Laboratory Animals; all procedures were approved by the Delaware State University Animal Care and Use Committee. All efforts were made to minimize animal numbers and distress. We used GFAP-tTA (Jackson Lab 005964) mice mated to TetO-hTDP Δ NLS (Jackson Lab 014650) mice to conditionally overexpress nuclear localization-signal deficient mice (Virginia Lee, Perelman School of Medicine, University of Pennsylvania). Pups were weaned from parents approximately 20 days after birth. Transgene was not suppressed through this tetOff system during development (no doxycycline was added to the diet). Animals were housed with littermates, and had free access to water and food. Animals were identified by piercing a hole in the ears relative to the cages and a small piece of the tail was cut for genotyping via PCR. Primers used to identify animals containing the TetO-hTDP Δ NLS construct are Forward -5' -TTGCGTGACTCTTTAGTATTGGTTTGA 3' and Reverse -5'CTCATCCATTGCTGCTGC 3'. Primers used to identify animals containing the GFAP-tTA construct are Forward -5'CGCTGTGGGGCATTCTTTACTTTAG 3' and Reverse- 5'CATGTCCAGATCGAAATCGTC 3'. Animals that were positive for both TetO-hTDP Δ NLS and GFAP-tTA in addition to littermate controls were the focus of this study.

3.2 Primary Cortical Neuron Cultures

Dissections were performed on late embryonic stage fetuses (approximately E₁₇-E₁₉). Expecting female mice were anesthetized with carbon dioxide and a sagittal cut was made through the abdominal cavity to expose the placenta and fetuses were removed. Fetuses were

placed in HBSS while dissections were being performed. Cortices were dissected and placed in plating media at 4°C while genotyping/PCR was performed. After genotyping, cortices of the same genotype were pooled together. Meninges were removed and cortices were placed in ice cold HBSS. Next, cortices were spun down at 300 x g for 5 minutes. HBSS was aspirated and HBSS with trypsin/EDTA was added to the tube and placed in 37°C for ten minutes. Cortices were spun down at 300 x g for 5 minutes. HBSS and trypsin mix was aspirated and DMEM with 10% horse serum, 10% fetal bovine serum and 1% penicillin/streptomycin was used to dissociate the cortices. Next the cortices were strained in a 70 micron cell strainer and were ready to be plated. 20,000 cells per well were plated on PDL coated coverslips in 24 well-plates in plating media for 45 minutes. Plating media was removed and replaced with neurobasal media supplemented with B27 (Invitrogen) and 0.5mM L-glutamine. For maintaining the cortical neuron cultures, half media changes were performed every two days.

a. Immunocytochemistry

After ten days, the media was removed and cells were washed with PBS. After 5 minutes, PBS was aspirated and cells were fixed with 4%PFA in 1X PBS for 15 minutes. Next PFA was aspirated and 5% BSA with 0.3% Triton-X 100 in 1X PBS was added for an hour for blocking. Primary antibodies: GFAP 1:1000(CST), TDP-43 1:500(Genscript), TDP-43 1:1000(Genscript), hTDP-43 1:5000(Abnova), β -III tubulin 1:1000 (CST) were incubated in 5% BSA with 0.3% Triton X-100 overnight at 4°C. The following day, slides were washed three times for 10 minutes each with PBS and incubated at room temperature for one hour with secondary Alexa-fluor antibodies (488 or 555) in 5%BSA with 0.3 Triton X-100 in 1X PBS. Coverslips were washed three times for 10 minutes each with PBS and were mounted using DAPI Fluoromount-

G (SouthernBiotech, Birmingham, AL). Images were taken using Nikon Eclipse *Ni* (Melville, NY), Nikon Intensilight C-HGFI (Melville, NY), NIS-Elements Software (Melville, NY).

3.3 Radial Arm Maze Test

An eight arm radial maze was used in a room with visual clues to test spatial short term and long term memory (schematic of radial arm maze found in Appendix A). The night prior to testing, the animal was food deprived. On test day, animals were placed in the testing room at least an hour before a 15-minute habituation trial. During the habituation trial, one of the eight arms was baited with the animal's regular diet. The animal was initially placed in the center of the radial arm maze facing away from the baited arm and was allowed to explore. In between each test subject, the maze was cleaned thoroughly with ethanol. After all test subjects were recorded in the habituation trial, short term memory was explored by returning each animal to the radial arm maze with the same baited arm for 5-minutes. That night, animals were food deprived again. 24-hours later, animals were placed in the testing room at least one hour before long term memory testing for 5-minutes per animal. All trials were recorded through a camera mounted above maze and animal body position and head position was recorded by automatic video tracking (ANY-maze, Stoelting Co). Modified protocol from Brown & Giumetti, 2006.

3.4 Y Maze Test

A Y-Maze with three identical arms made of sheet metal placed at 120 angles to each other was used in a room with visual clues to test working memory (schematic of Y-Maze found in Appendix A). One arm was blocked to prevent the mouse from entering novel arm. The mouse was initially placed in the arm adjacent to the known and novel arm and was allotted a 10-minute acquisition period to explore the known arm. In between each test subject, the maze was cleaned

thoroughly with ethanol. After all test subjects were recorded in an acquisition trial, sheet metal was removed and the novel arm was open for exploration for the retention trial for five minutes. All retention trials were recorded through a camera mounted above maze and animal position was recorded by automatic video tracking (ANY-maze, Stoelting Co). Modified protocol from Alfieri, Silva, & Igaz, 2016.

3.5 Immunohistochemistry

Animals used in behavior studies were anesthetized using carbon dioxide then were fixed with 4% paraformaldehyde via trans-cardial perfusions. Whole brain and spinal cord was extracted and post-fixed in 4% paraformaldehyde. One coronal cut was made through the brain and it was embedded in paraffin. 6 micron sections were cut using a microtome and sections were ready for staining. Slides were deparaffinized in xylene for four minutes and rehydrated in 100% EtOH, 95% EtOH, 70% EtOH, 50% EtOH and were subject to antigen retrieval by using 0.01M sodium citrate. Slides were placed in constant flow of deionized water for fifteen minutes prior to an hour of blocking with 5% BSA with 0.3% Triton X-100 in 1X PBS.

a. Immunofluorescence

Primary antibodies: Myelin Basic Protein 1:500(CST), GFAP 1:1000(CST), TDP-43 1:500(Genscript), TDP-43 1:1000(Genscript) were incubated in 5% BSA with 0.3% Triton X-100 overnight at 4°C. The following day, slides were washed three times for 10 minutes each with PBS and incubated at room temperature for one hour with secondary Alexa-fluor antibodies (488 or 555) in 5%BSA with 0.3 Triton X-100. Slides were washed three times for 10 minutes each with PBS and were mounted using DAPI Fluoromount-G (SouthernBiotech, Birmingham, AL).

Cresyl Echt Violet

After deparaffinization and rehydration, slides were washed for 5 minutes in distilled water. Then they were placed in CEV solution for 3 mins. The slides were then rinsed in distilled water for 5 minutes. Slides were then counterstained in hematoxylin for 30 seconds and rinsed again in distilled water for 4 minutes. The slides were then dipped in 1% acid alcohol, rinsed for 2 minutes in distilled water, dipped in ammonia water 8 times and rinsed for the last time in distilled water for 3 minutes. Finally, slides were dehydrated to xylene and coverslipped with permount mounting media.

3.6 RNA Extraction

Animals were anesthetized with CO₂. The spinal cord of each animal was removed and using a syringe filled with PBS inserted at the caudal end of the spinal column, the spinal cord was removed and immediately homogenized in 0.5mL of ice cold TRIzol (Invitrogen). Spinal cord samples were frozen at -80° overnight. Thaw the samples on ice when ready to isolate RNA. Prior to isolating RNA, work benches, centrifuges and pipettes should be cleaned with RNaseZAP RNase Decontamination Solution to prevent contamination. To further lyse the spinal cord, add 0.2mL of chloroform. Vigorously shake for 30 seconds then immediately incubate for 3 minutes at room temperature. Centrifuge the samples at 4°C for 15 minutes at 12,000 x g. Carefully transfer the aqueous phase to a new Eppendorf tube. To precipitate the RNA, add 1mL of isopropanol to the new Eppendorf tube and incubate at room temperature for 10 minutes. Centrifuge the samples at 4° for 10 minutes at 12,000 x g. Discard the supernatant, RNA precipitate is formed in the pellet. Re-suspend pellet in 1mL of 75% ethanol, vortex for 5 seconds and centrifuge at 7500 x g for 5 minutes at 4°C. Discard the supernatant and allow pellet

to air dry. Solubilize the pellet in 50uL of RNase-free water. Measure RNA yield by using NanoDrop Lite (ThermoFisher, Waltham, MA). RNA was sent to Nemours/Alfred I. DuPont Hospital for Children (Wilmington, DE) for processing. Data was analyzed using Affymetrix Expression Console Software (ThermoFisher, Waltham, MA).

3.7 Data Analysis

Immunofluorescence was quantified, analyzed and graphed using Prism 7 (GraphPad Software, Inc.). Behavior data was quantified, analyzed and graphed using Prism 7 (GraphPad Software, Inc.). Data are expressed as mean values \pm SEM. Two-sample T-tests were used to analyze β III-tubulin fluorescence intensity, GFAP fluorescence intensity, radial arm maze behavior studies and y-maze behavior studies. P values from statistical tests that were identified as $p < 0.05$ were considered statistically significant.

CHAPTER 4: RESULTS

4.1 Non-cell autonomous changes are observed *in vitro*

hGFAP-tTA mice were bred with TetO-hTDP-43 Δ NLS mice, E₁₇-E₁₉ pups were dissected and cortices were used for cortical neuron cultures to visualize the effects of a defective nuclear localization signal of TDP-43 in astrocytes. We observed the presence of both human specific TDP-43(hTDP-43) and GFAP in astrocytes (Figure 1). WT cultures showed the presence of GFAP in astrocytes and the absence of hTDP-43 since the transgene was not expressed. GFAP/TDP-43 Δ NLS cultures showed hTDP-43 expression in the cytoplasm of astrocytes. We expected to see co-localization of the two proteins since that they co-habited the cytoplasm but they stained individual astrocytes. hTDP-43 staining revealed a different morphology of the astrocytes. They are not long and fibrous compared to GFAP-positive astrocytes in WT cultures.

Presence of hTDP-43 expression selectively in some astrocytes but not all astrocytes by using the hGFAP promoter raised some concerns regarding expression of both GFAP and TDP-43. Since that astrocytic TDP-43 Δ NLS is being driven by the hGFAP promoter during development, competition for astrocytic expression of GFAP and TDP-43 may be present which is why co-localization was not observed *in vitro*. We also observed punctate staining of hTDP-43 in astrocytes rather than diffuse staining that is seen in GFAP-positive astrocytes in the WT culture. Punctate staining of TDP-43 could be representative of TDP-43 accumulation and aggregation due to a defective nuclear localization signal. Therefore astrocyte morphology and composition is different in GFAP/TDP-43 Δ NLS cultures. Since that we were seeing these

changes with hTDP-43 expression, we next wanted to observe total TDP-43 staining in cortical neuron cultures.

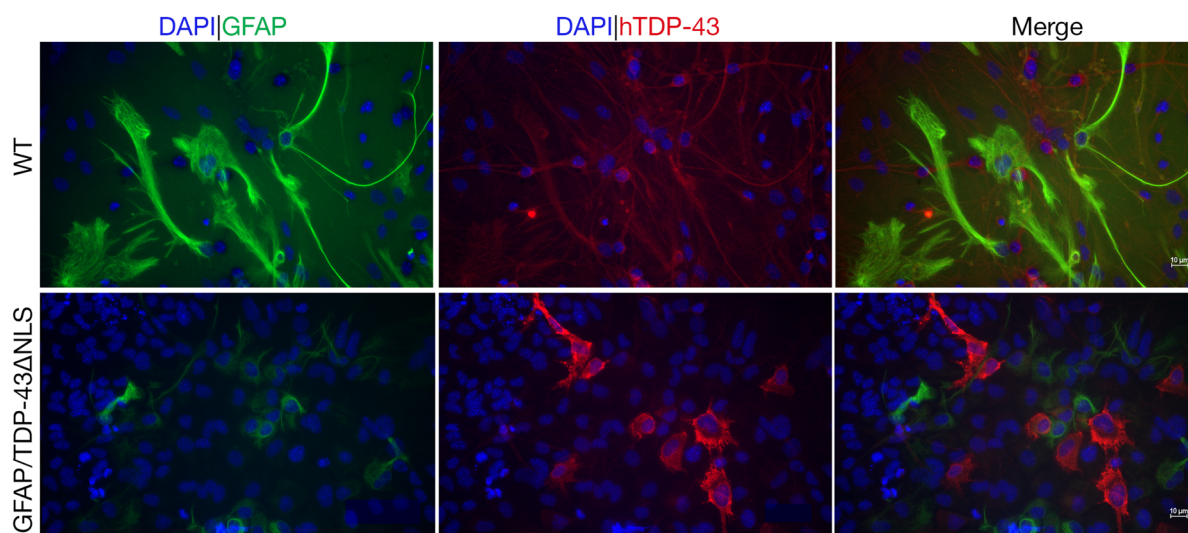


Figure 1. hTDP-43 localizes to the cytoplasm of GFAP/TDP-43 Δ NLS astrocytes

hGFAP promoter selectively expresses hTDP-43 in astrocytes found in primary cortical neuron/astrocyte co-cultures from mice brain cortices which were dissected at E₁₇-E₁₉. Cells were grown ten days in vitro prior to fixation and staining. GFAP staining (green) shows presence of GFAP-positive astrocytes in both WT and GFAP/TDP-43 Δ NLS cultures. Punctate staining of hTDP-43 (red) is observed in GFAP/TDP-43 Δ NLS astrocytes opposed to diffuse and fiber-like staining of astrocytes in WT. *Magnification 400X*

In primary cultures, we observed total TDP-43 and GFAP expression (Figure 2). In the WT cultures, TDP-43 stained the nucleus and GFAP staining appears to be normal. In GFAP/TDP-43 Δ NLS cultures, TDP-43 stained the nucleus and cytoplasm. This was not abnormal because these cultures are not pure astrocyte cultures. The presence of nuclear TDP-43 suggests that TDP-43 is present in neurons and that the function of TDP-43 in neurons may have limited effects. The presence of cytoplasmic TDP-43 suggests that TDP-43 is present in astrocytes due to hGFAP promoter expressing hTDP-43 Δ NLS. The absence of GFAP expression in astrocytes that are TDP-43-positive suggests that TDP-43 may be modulating GFAP by

inhibiting expression or decreasing expression in astrocytes via possible changes in splicing or a toxic gain of protein accumulation of TDP-43 in the cytoplasm. Once again, these proteins may also be competing for astrocytic cytoplasmic expression due to TDP-43 Δ NLS being expressed during development. In Figures 1 and 2, astrocyte morphology and normal expression of GFAP was disturbed due to expression of TDP-43 Δ NLS via hGFAP promoter.

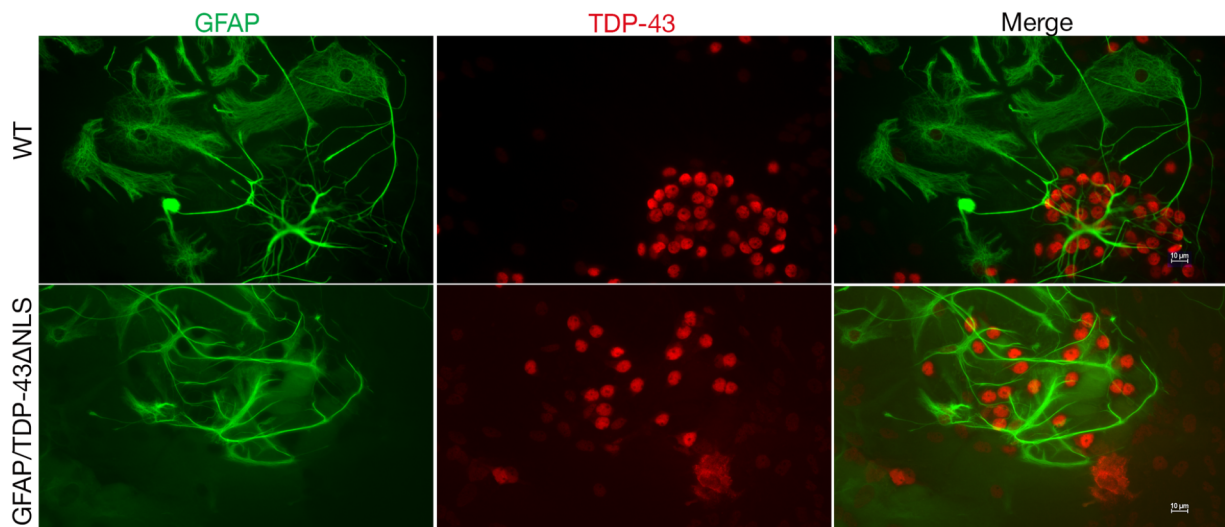


Figure 2. TDP-43 is present in nucleus and cytoplasm *in vitro*

Primary cortical neuron/astrocyte co-cultures from mice brain cortices which were dissected at E₁₇-E₁₉. Cells were grown ten days *in vitro* prior to fixation and staining. GFAP staining (green) shows presence of GFAP-positive astrocytes in both WT and GFAP/TDP-43 Δ NLS cultures. TDP-43 (red) usually present in the nucleus is present in both the nucleus and cytoplasm in primary cultures. *Magnification 400X*

Since that GFAP expression was disturbed, we wanted to see if the neurons in primary culture were affected by astrocytic expression of TDP-43 Δ NLS. We hypothesized that TDP-43 Δ NLS would reflect non-cell autonomous changes in neurons. Prior to staining, we observed neuronal changes under microscope and observed the proliferation of non-neuronal cells. To explore this concept we visualized astrocytes and neurons by staining with GFAP and β III-tubulin (Figure 3A). We noticed that β III-tubulin expression was abundant in WT cultures.

Neuron structure consisted of complex branching and well-developed complex networks in WT staining but we did not observe the same networking in GFAP/TDP-43 Δ NLS cultures. We quantified the fluorescence intensity of β III-tubulin (Figure 3B) and found that there was a significant decrease in GFAP/TDP-43 Δ NLS cultures (Two sample T-test, $p < 0.05$). This non-cell autonomous change is representative of neuronal degeneration when TDP-43 Δ NLS is expressed in astrocytes. Ironically, when GFAP was quantified, there was no significant difference (Figure 3C).

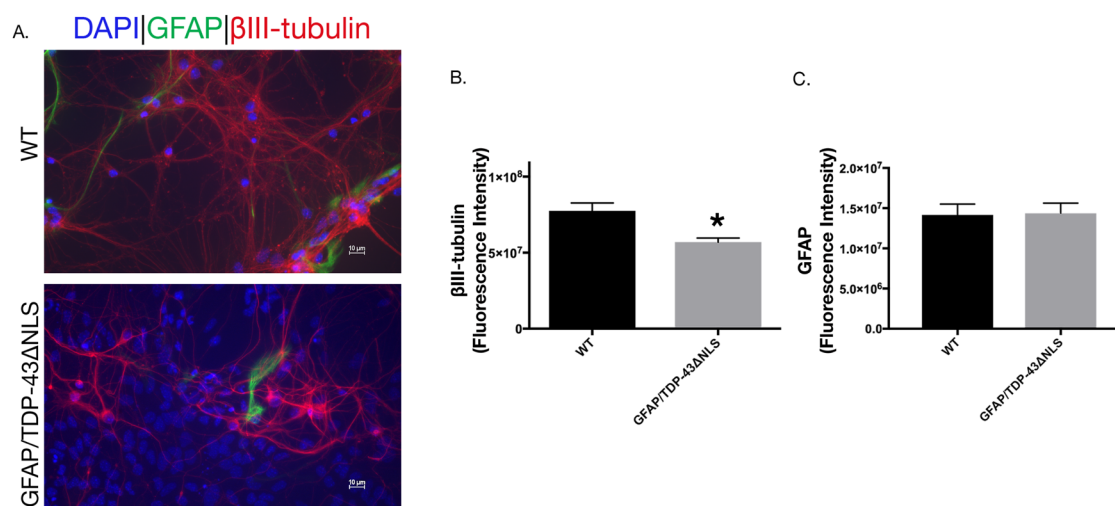


Figure 3. Neuron structure changes are observed in GFAP/TDP-43 Δ NLS primary cultures
 (A) Neurons from primary cortical neuron cultures (mice ages E₁₇-E₁₉ and cells grown for 10 days prior to fixation and staining) show a change in neuron structure seen as neurite outgrowth and fluorescence intensity. *Magnification 400X* (B) Fluorescence of β III-tubulin was significantly decreased in GFAP/TDP-43 Δ NLS cultures (Two-sample t-test, * = $p < 0.05$, WT n=13 and GFAP/TDP-43 Δ NLS n=13) (C) Fluorescence of GFAP in GFAP/TDP-43 Δ NLS cultures was not significant compared to WT cultures (Two-sample t-test, * = $p < 0.05$, WT n=13 and GFAP/TDP-43 Δ NLS n=13)

4.2 Astrocyte specific expression of TDP-43 Δ NLS induces memory deficits

With selective expression of TDP-43 in astrocytes inducing neurodegeneration *in vitro* and the importance of astrocytes in neurogenesis in the hippocampus and long-term potentiation,

we hypothesized that our model of astrocytic TDP-43 would induce memory deficits *in vivo*. To explore this hypothesis, we used an 8 arm radial maze to test spatial memory. Two-month old mice were food deprived (16 hours) and allowed to explore the maze for 15 minutes. Each animal entered the baited arm and found the reward within the 15-minute trial. An hour after the initial trial, animals were tested for short term memory. We allowed the animals 5 minutes to explore the maze and their activity such as time spent in each arm was tracked. We show that GFAP/TDP-43 Δ NLS animals spent significantly less time immobile in the baited arm in this short term memory experiment (32.06 ± 11.69 . Two sample t-test, $*=p < 0.05$, WT n=5, GFAP/TDP-43 Δ NLS n= 6) (Figure 4A).

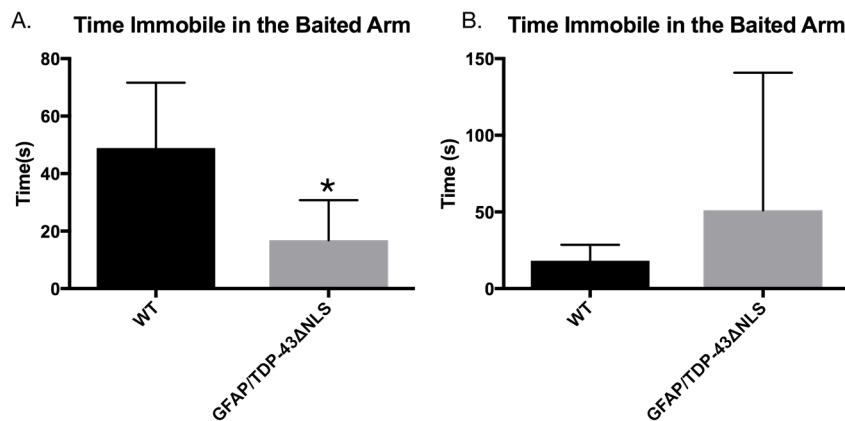


Figure 4. Spatial memory deficits are observed in 2-month old GFAP/TDP-43 Δ NLS mice. (A) 1 hour after the acquisition trial, GFAP/TDP-43 Δ NLS animals spent less time immobile in the baited arm. (B) 24 hours after the short term trial, there was no significant difference between time immobile for both animal sets. (Two-sample t-test, $*=p < 0.05$, WT n = 5, GFAP/TDP-43 Δ NLS n= 6)

Twenty-four hours later, we tested long term memory with the food-deprived animals. Again, we allowed the animals 5 minutes to explore and their activity was tracked. We found no change in immobile time spent in the baited arm (32.85 ± 40.72 . Two sample t-test, $*=p < 0.05$, WT n=5, GFAP/TDP-43 Δ NLS n= 6) (Figure 4B). GFAP/TDP-43 Δ NLS error bars are larger

(Figure 4B) but we did not remove that test subject because we had a small sample population.

We also tested exploratory behavior and working memory in 2-month old GFAP/TDP-43 Δ NLS mice. For this experiment, we used a Y-maze where mice were initially exposed to only one arm (known) and were later exposed to both the known arm and a novel arm. Animal activity was tracked in the trial where the animal was exposed to the known and novel arm. Behavior changes were observed in GFAP/TDP-43 Δ NLS test subjects.

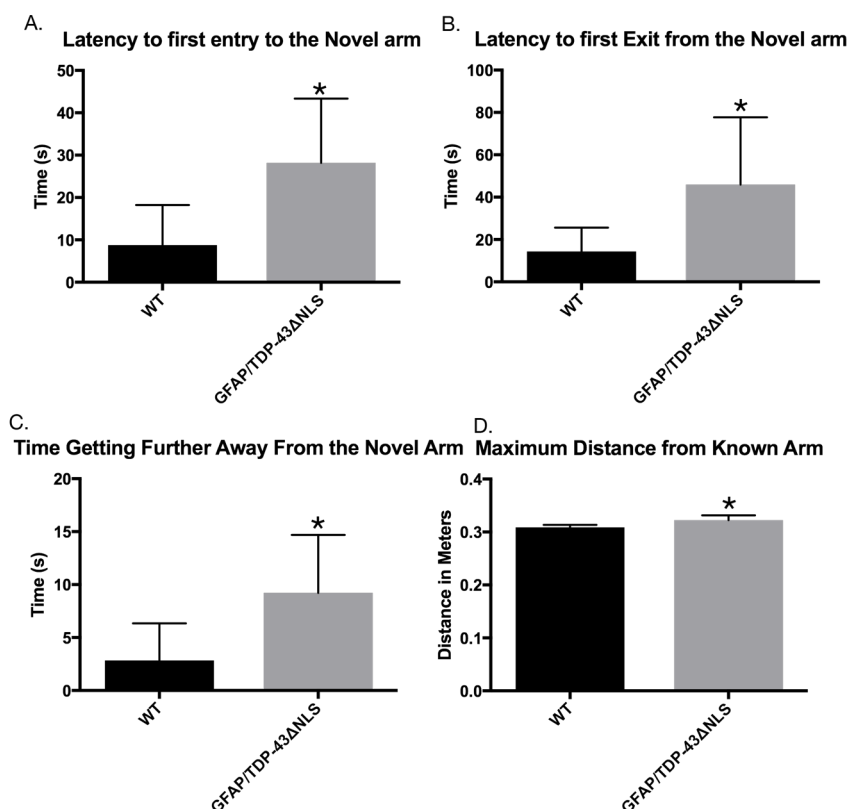


Figure 5. Exploratory behavior and working memory changes are observed in 2-month old GFAP/TDP-43 Δ NLS mice. GFAP/TDP-43 Δ NLS model shows deficits in exploratory behavior and working memory. Naturally, mice explore new environments. In the GFAP/TDP-43 Δ NLS model, (A) animals spent a significantly larger amount of time exploring the known environment; (B) animals spent a significantly larger amount of time their first time visiting the novel arm before exiting; (C) animals spent significantly larger amount of time moving away from the novel arm; and (D) animals spent significantly larger maximum distance away from the known arm. (Two-sample t-test, * = $p < 0.05$, WT $n = 5$, GFAP/TDP-43 Δ NLS $n = 6$)

Ideally, animals tend to explore new areas and alternate between locations quite frequently in a scenario where they can exercise exploratory behavior and working memory. In GFAP/TDP-43 Δ NLS model, upon starting the trial, these animals took about 30 seconds to enter the novel arm (Figure 5A). This was a significantly longer period of time compared to WT animals. Ironically, these animals also took a significantly longer period of time to first exit the novel arm (Figure 5B), (31.58 ± 13.79 . Two sample t-test, $*=p < 0.05$, WT n=5, GFAP/TDP-43 Δ NLS n= 6).

This can mean that animals spent more time exploring in the novel arm or took more time to orient itself in the new location. Animals spent a significantly longer period of time moving further away from the novel arm and returning to the known arm or start arm, (Figure 5C), (6.37 ± 2.716 . Two sample t-test, $*=p < 0.05$, WT n=5, GFAP/TDP-43 Δ NLS n= 6).

It was also tracked that GFAP/TDP-43 Δ NLS animals moved further away from the known arm (Figure 5D), (0.0134 ± 0.00422 . Two sample t-test, $*=p < 0.05$, WT n=5, GFAP/TDP-43 Δ NLS n= 6). Animal behavior was affected by manipulation of astrocytic TDP-43 but it is essential to note that motor coordination or motor function was not affected. Animals were mobile and did not show inability or difficulty moving. Working memory, spatial short term memory and exploratory behavior was affected.

4.3 TDP-43 Δ NLS induces abnormal expression in brain and spinal cord

We wanted to evaluate the quality of the brains and spinal cords of animals from the behavior study so we sacrificed the animals preserved the brains and spinal cords using 4%PFA. Spinal cords of 2-month old and 6-month old animals were stained with Cresyl Echt Violet (CEV). At 2 month's old, the spinal cord structure as a whole looks normal. Motor neurons

under 400X magnification display a crescent, sickle morphology, rather than a healthy pyramidal morphology which represents loss of nissl-substance (Figure 6A). These motor neurons still retain the large cell bodies indicative of motor neuron cell morphology but appear to be degenerating. In 6-month old mice, neurons appear to be dead, represented by dark purple and indicated with black arrows (Figure 6B).

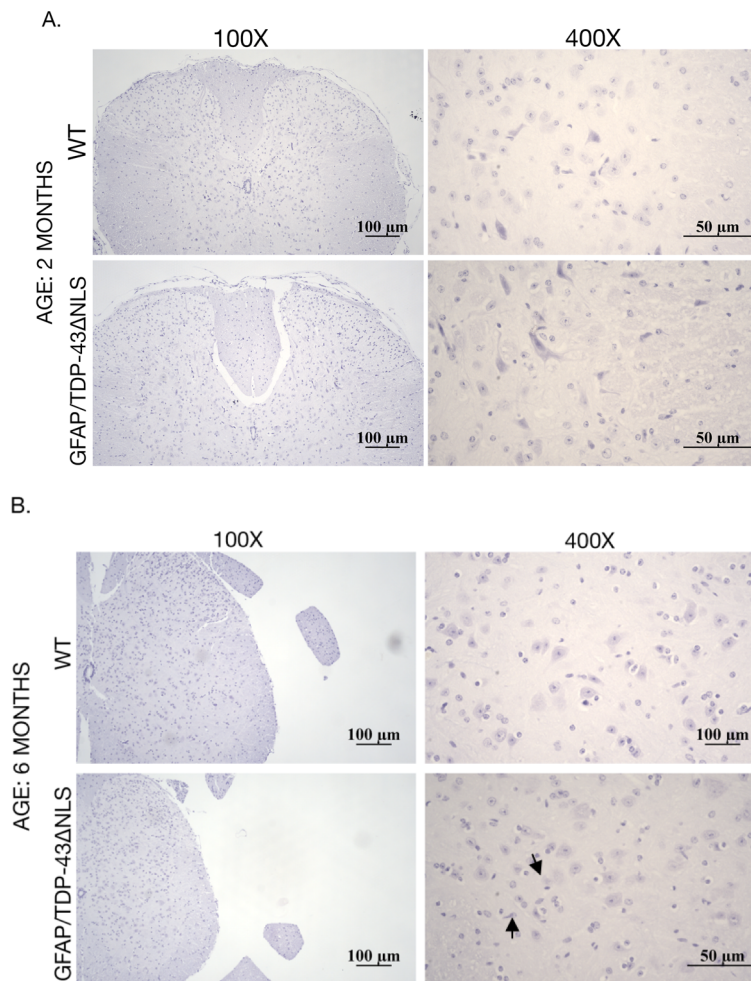


Figure 6. Nissl Stain reveals changes in motor neuron structure in GFAP/TDP-43ΔNLS mice
 Transverse sections of the spinal cord show changes in motor neuron morphology and a change in structure indicative of early motor neuron degeneration. GFAP/TDP-43ΔNLS mice in both age groups show change in motor neuron morphology with preserved large cell bodies. (A) 2-month old littermates (n=3 per genotype). (B) 6-month old littermates (n=2 per genotype).

To further evaluate the effects of TDP-43 Δ NLS on the brain and spinal cord, we stained for TDP-43 and GFAP. We expected to see TDP-43 expression in majority of the astrocytes *in vivo* by using the hGFAP promoter but surprisingly in the dentate gyrus more astrocytes were GFAP positive and TDP-43 negative (Figure 7A and Figure 7B). Taking a closer look, astrocytes that were TDP-43-positive appeared with larger cell bodies and complex branching. Astrocytes GFAP-positive appeared slim and longitudinal with minimal branching. This distinct staining was seen in both 2-month old mice and 6-month old mice.

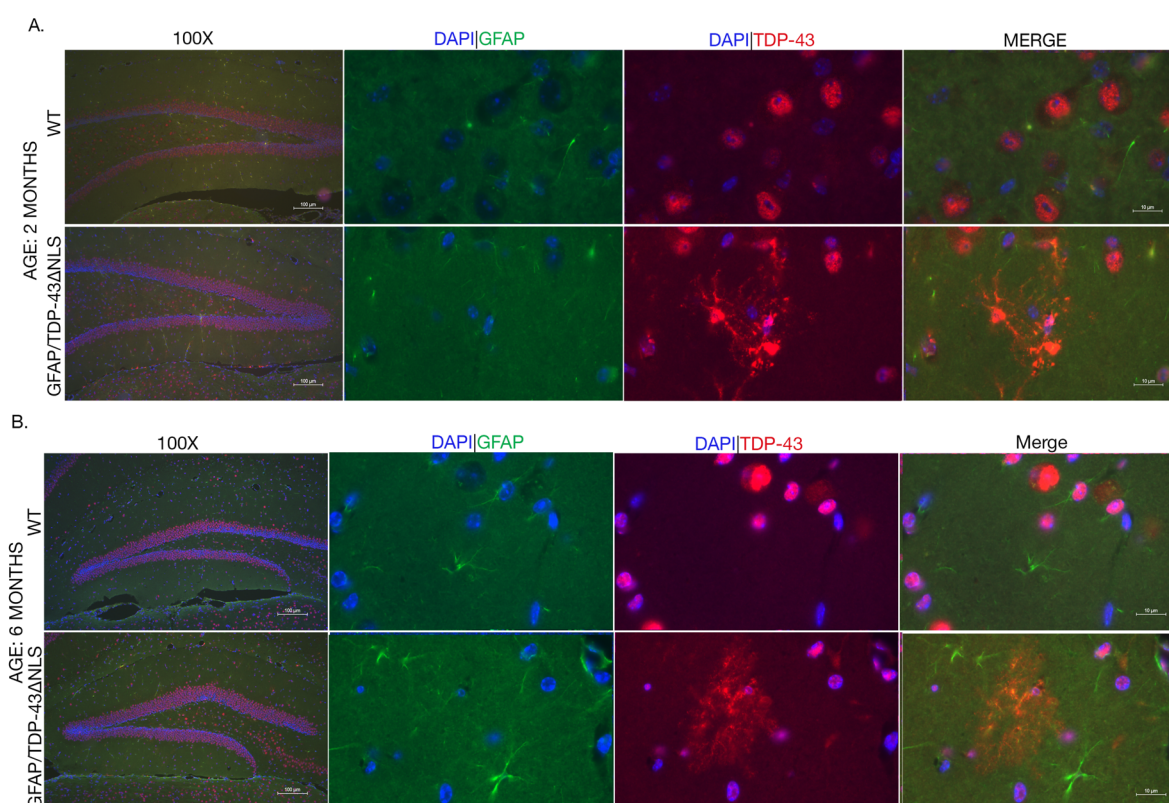


Figure 7. Expression of TDP-43 Δ NLS exposes heterogeneity of astrocytes in dentate gyrus

In 2-month old and 6-month old mice, astrocytes positive for TDP-43 are negative for GFAP. Observed in the dentate gyrus are astrocytes with complex branching and large cell bodies negative for DAPI and minimal expression of GFAP. (A) 2-month old littermates (n=3 per genotype). (B) 6-month old littermates (n=2 per genotype). In panel 1, magnification is 100X. In panels 2-4, magnification is 1000X.

Once again, the question of promoter activity and the downstream effects that it plays on GFAP

expression surfaces. GFAP and TDP-43 may be competing to be expressed in the astrocytes since that TDP-43 Δ NLS was expressed during development. GFAP is present and uniformly expressed throughout the dentate gyrus in both 2-month old and 6-month old mice.

Abnormalities of astrocytic expression via immunofluorescence were also seen in the spinal cord.

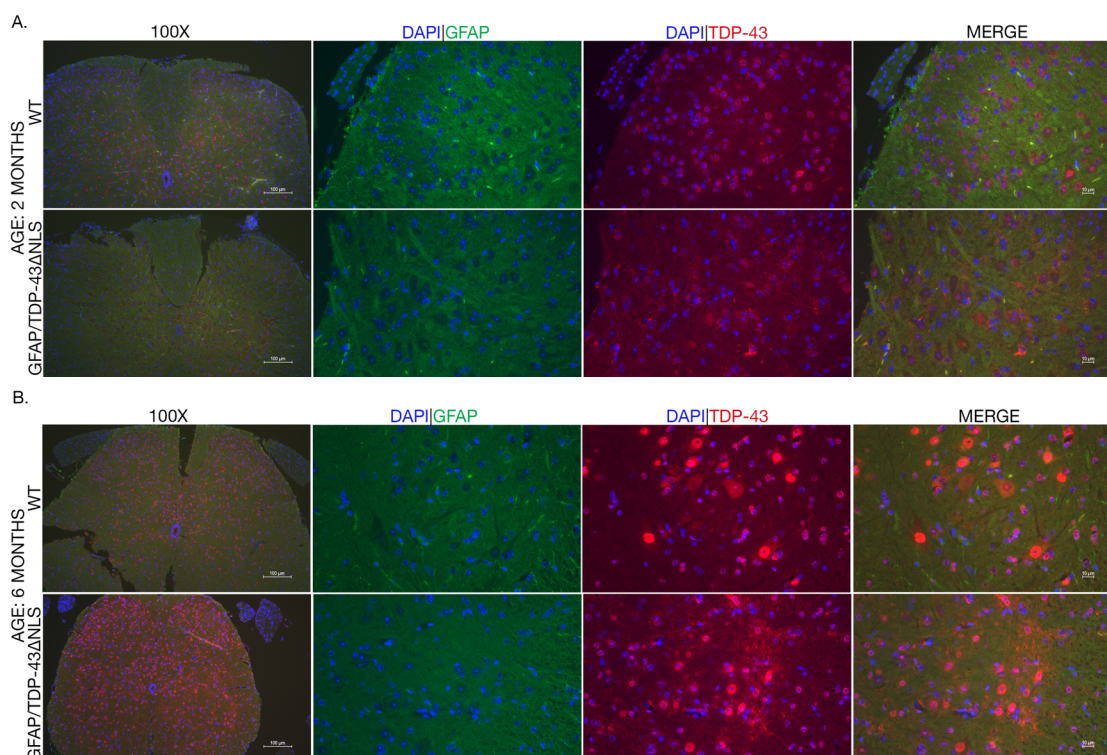


Figure 8. TDP-43 Δ NLS induces increase of TDP-43 correlated with age in spinal cord

In vivo GFAP and TDP-43 staining in the spinal cord of 2-month old and 6-month old show age dependent increase of TDP-43 in the grey matter of the spinal cord. GFAP(green) is present and localized to white matter in the spinal cord. TDP-43(red) shows punctate staining in GFAP/TDP-43 Δ NLS spinal cords in 2-month old and 6-month old age groups but is increased drastically in 6-month old NLS mice compared to WT littermates. (A) 2-month old littermates (n=3 per genotype). (B) 6-month old littermates (n=2 per genotype). In panel 1, magnification is 100X. In panels 2-4, magnification is 400X.

Expression of GFAP in the spinal cord is generally localized to white matter and nuclei are centralized in the grey matter, but in GFAP/TDP-43 Δ NLS spinal cords exclusively expressing TDP-43 Δ NLS in astrocytes a new pattern of organization is formed. GFAP-positive

astrocytes are relatively expressed in white matter appearing as diffuse longitudinal staining. At 2-months of age, TDP-43 is seen in the spinal cord localized to nuclei as well as astrocytes. (Figure 8A) At 6-months of age, TDP-43 is highly expressed in the grey matter of the spinal cord (Figure 8B). Spinal cord from 6-month old GFAP/TDP-43 Δ NLS mice show a dramatic increase in the expression of TDP-43 as a result of expression of astrocytic TDP-43 Δ NLS. This age dependent change of expression for TDP-43 may be indicative of severe memory deficits that were not observed in 2-month old mice in the y-maze and radial arm maze.

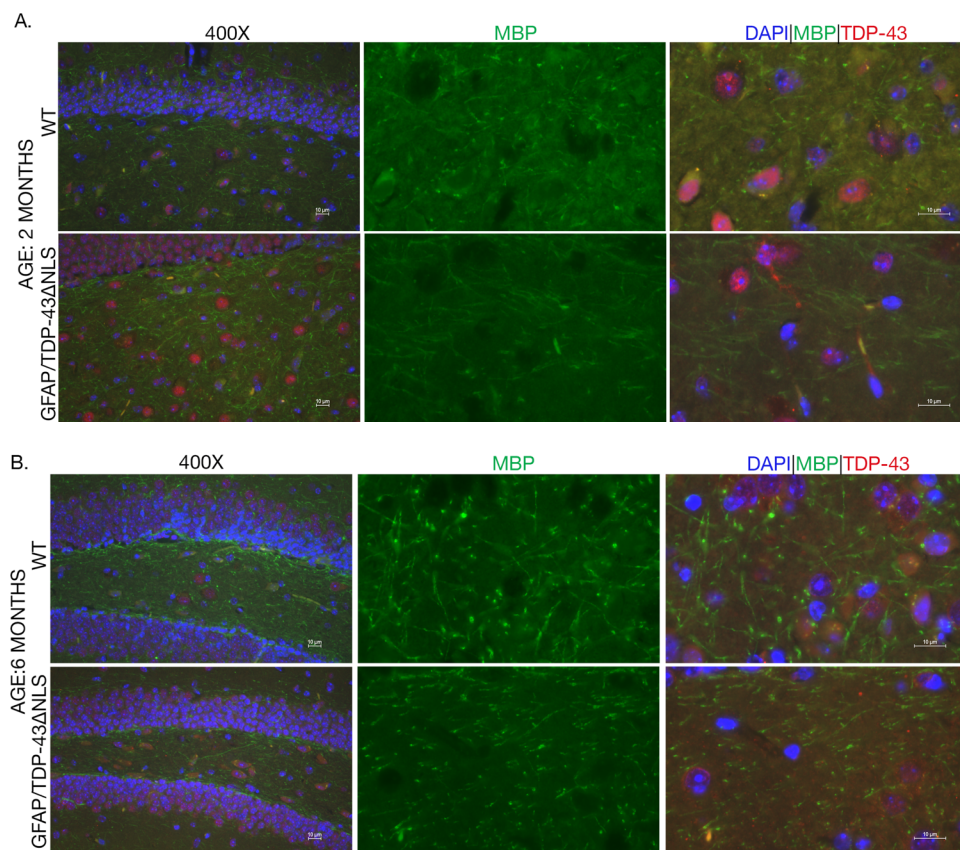


Figure 9. Myelin basic protein expression pattern is altered in dentate gyrus due to astrocytic expression of TDP-43 Δ NLS

Myelin basic protein(green) expression is affected by astrocytic expression of TDP-43 Δ NLS in an age-dependent manner in the dentate gyrus. Overtime, the pattern changes Sections are counterstained with TDP-43(red) and DAPI(blue). (A)2-month old littermates (n=3 per genotype). (B)6-month old littermates (n=2 per genotype). In panel 1, magnification is 100X. In panels 2-4, magnification is 400X.

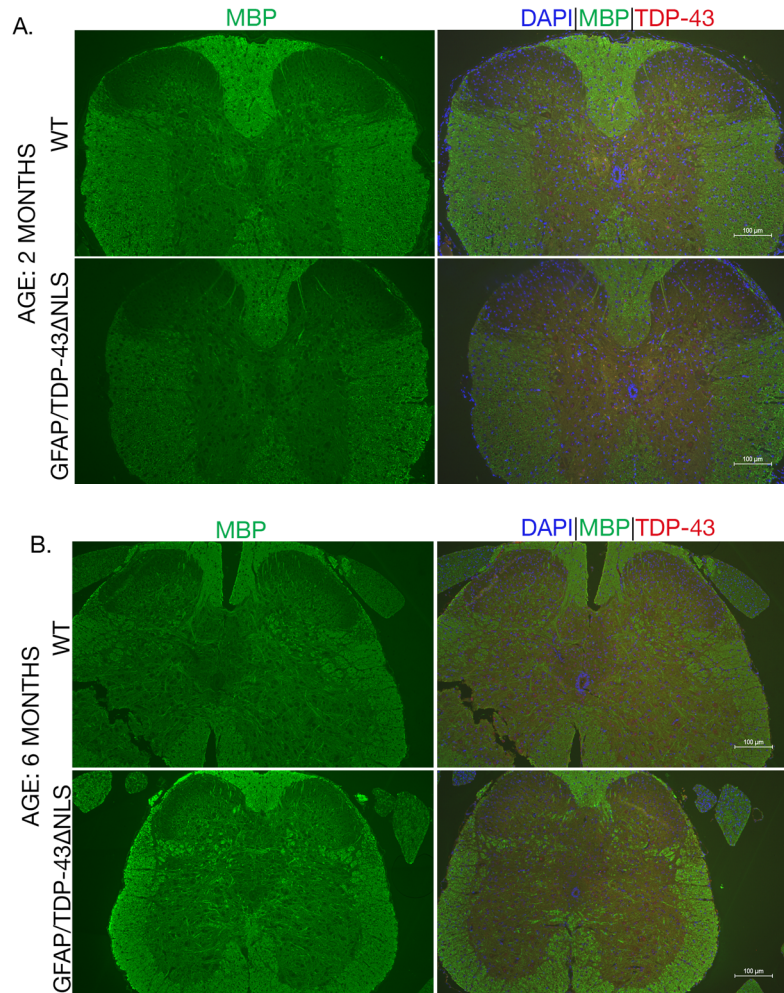


Figure 10. Grey matter of spinal cord shows changes in myelin basic protein expression
 Myelin basic protein(green) expression shows progressive changes in the grey matter of the spinal cord. Sections are counterstained with TDP-43(red) and DAPI(blue). (A)2-month old littermates (n=3 per genotype). (B)6-month old littermates (n=2 per genotype). Magnification is 100X.

4.4 GFAP/TDP-43 Δ NLS mice show age dependent change in Myelin Basic Protein

Expression

Since that we saw these changes in the grey matter and white matter, we hypothesized that myelin basic protein would be affected in an age-dependent manner due to the astrocytic expression of TDP-43 Δ NLS. We stained 2-month and 6-month old brains and spinal cord sections with MBP and focused on the dentate gyrus. We see that at 2-months old, there is a

decrease in myelin basic protein expression in the hippocampus. We also see a change in myelin basic protein expression pattern (Figure 9A). This trend is also seen in 6-month old GFAP/TDP-43 Δ NLS mice (Figure 9B). In the spinal cord, expression of MBP looks evenly distributed in white matter. In the grey matter, there is low expression of MBP (Figure 10A). There is also a different expression pattern in the grey matter of the spinal cord. MBP is prominent in the ventral horn of the spinal cord in WT mice, while there is a decrease and low expression of MBP in the ventral horn of the spinal cord in GFAP/TDP-43 Δ NLS (Figure 10B).

4.5 Exploration of gene expression and splicing via exon array

Category	Total Number of Genes	Genes expressed in both conditions	Genes expressed in only WT	Genes expressed in only GFAP/TDP-43 Δ NLS	Genes not expressed in both
Coding	10628	9919	204	121	384
Complex	15644	15324	103	67	150
Non-Coding	36581	35100	449	269	763
Other	27	0	0	0	27
Pseudogene	2711	2656	23	10	22
Ribosomal	155	155	0	0	0
Unassigned	24	22	1	1	0

Table 1. Overview of TDP-43 splicing in GFAP/TDP-43 Δ NLS model

RNA from 2-month old mice spinal cords was extracted and sent for processing. This table breaks down how many genes were affected by alternative splicing activity. (WT n=3, GFAP/TDP-43 Δ NLS n=3)

RNA from 2-month old mice was used for an exon array to analyze TDP-43 splicing index, gene fold changes, and group (i.e coding, complex, noncoding, pseudogene and ribosomal) (Table 1). This table breaks down the alternative splicing activity that occurred by astrocytic expression of TDP-43 Δ NLS. Astrocytic TDP-43 spliced a total of 65,770 genes. Of the 10,628 coding genes that were spliced, MAPKKK, synaptotagmin II, doublecortin domain, hairless, astrotactin 1 were included. Reln, GFAP, Myef2 (MBP repressor), Grin1 and Grin3a and Nsmf (genes that code for NMDA) and others are complex gene that was affected by TDP-43 splicing. The splicing index of GFAP was -1.12, -1.11, -1.08 and 1.06 and the gene fold change was 1.11. The splicing index is representative of exons included or excluded by alternative splicing (ThermoFisher.).

CHAPTER 5: DISCUSSION

As we begin to look at the effects of astrocytic TDP-43 Δ NLS *in vitro*, we immediately notice that astrocytes appearing in our model are different from the fibrous, star-like morphology that is commonly seen. By staining with two TDP-43 antibodies (both human specific and total TDP-43), it appears that with hTDP-43, shuttling properties of TDP-43 in astrocytes are minimal and majority of TDP-43 is found in the cytoplasm (Figure 1)(Y. M. Ayala et al., 2008). These results verify that the mutation (Δ NLS) is expressed and TDP-43 normal localization is defective. The antibody that recognizes both mouse and human TDP-43 stains the nucleus of neurons and the cytoplasm of astrocytes (Figure 2). The morphology of the astrocytes *in vitro* was a result of nuclear clearance of TDP-43 (Winton et al., 2008). Nuclear clearance in glia is also present in ALS and FTLN cases(Winton et al., 2008). Models that recapitulate TDP-43 proteinopathies generally start at the upstream effect, opposed to our model which creates the pathology by inducing TDP-43 Δ NLS in astrocytes (review in Tsao et al., 2012). We did not confirm that TDP-43 cytoplasmic aggregates are present or absent, but the presence of cytoplasmic TDP-43 contributes to the understanding of proteinopathies.

It is evident that astrocytic expression of TDP- 43 Δ NLS during development results in accumulation of hTDP-43 and total TDP-43 in the cytoplasm. Since that GFAP is expressed relatively late during development in mice(E_{17.5}-E_{18.5}), it is very likely that TDP-43 and GFAP are competing to be expressed in astrocytes (reviewed in Molofsky et al., 2012). This may be why the *in vitro* and *in vivo* studies show astrocytes that are TDP-43-positive while simultaneously GFAP negative (Figure 1, Figure 2 and Figure 8). GFAP-positive astrocytes

appeared to be minimal in number *in vitro* but when quantified there was no significant difference between the immunoreactivity of GFAP in GFAP/TDP-43 Δ NLS primary cultures compared to WT primary cultures (Figure 3C). Astrocytes in culture may be reactive and may be expressing high levels of GFAP to compensate for astrocytes that are TDP-43 negative. Co-localization was present *in vivo* in the dentate gyrus but was not present in every astrocyte that was TDP-43 positive. The different effects that were observed *in vitro* and *in vivo* may be due to a combination of factors such as expression during development, competition and alternative splicing activity.

Cell-autonomy and non-cell autonomous neurodegeneration effects have been observed in TDP-43 proteinopathies where mutations known to be a causative factor in inducing pathogenesis of neurodegenerative diseases are used in animal models or *in vitro* with iPSC's (Huang et al., 2014; A. Serio et al., 2013). Our model results in a non-cell neurodegeneration when TDP-43 Δ NLS is expressed in astrocytes (Figure 3). Astrocytes aid and support neurons in many ways such as transferring their mitochondria to neurons, neuroprotective functions such as reactive astrogliosis and secretion of neurotransmitters, neuromodulators, growth factors and other secretory molecules (Hayakawa et al., 2017; Yuan Liu et al., 2012; Verkhratsky, Matteoli, Parpura, Mothet, & Zorec, 2016).

TDP-43 expression in astrocytes had an effect on the expression of GFAP (known to be a major astrocyte marker), and will be further explored and validated through immunoblotting in future studies. Both *in vitro* and *in vivo* studies have shown co-localization of TDP-43 and GFAP in disease models (Huang et al., 2014; Lanciotti et al., 2013; Andrea Serio et al., 2013). The absence of GFAP-positive astrocytes and the presence of TDP-43-positive astrocytes

sparked an interest that TDP-43 Δ NLS expression causes alternative splicing and changes in RNA metabolism under the circumstances in our model (Y. M. Ayala et al., 2008; Tollervey et al., 2011). Initially through a proteomics screen we found that TDP-43 and GFAP interact in complex (this has not been validated through co-immunoprecipitation). There still may be a functional interaction between TDP-43 and GFAP such that when TDP-43 is overexpressed, we see a reduction of GFAP-positive astrocytes while maintaining immunoreactivity.

For astrocytes to be inactivated, there would be a total absence of GFAP. TDP-43 positive astrocytes were uniquely distinct in shape, composition, and complexity. TDP-43 astrocytes highly-resembled protoplasmic astrocytes due complex branching. Protoplasmic astrocytes are a type of GFAP-expressing astrocyte that are found in the central nervous system (Yuan Liu et al., 2012). They are known to develop dense connections with neurons and play a strong role in synapse activity (Stork, Sheehan, Tasdemir-yilmaz, & Freeman, 2015). We hypothesized that splicing activity was occurring and TDP-43 alternatively splices GFAP. GFAP and other genes affected may not be the specific binding targets of TDP-43 but they are a direct result of the inability of the mutant TDP-43 to relocate to the nucleus in astrocytes. TDP-43 is known to function through a self-regulating negative feedback loop by down-regulating its transcription levels (Youhna M Ayala et al., 2011). Therefore overexpression of TDP-43 by transgene hTDP-43 Δ NLS does not increase total amount of TDP-43 in cells. TDP-43 negative feedback loop will decrease expression in nucleus because expression TDP-43 in the cytoplasm is increased. Complex genes alternatively spliced by TDP-43 (Table 1), reveal that GFAP is spliced by TDP-43 at different splicing indices and induce different fold changes. GFAP may still be a functioning protein although expression level is decreased *in vitro* and *in vivo*.

GFAP expression in the spinal cord revealed low expression of GFAP but support the idea of heterogeneity of astrocytes. First, analysis of 2-month old spinal cord using CEV stain shows dying motor neurons similar to what is seen in ALS and FTLN-TDP (Blitterswijk et al., 2014). Motor neurons were longitudinal rather than diamond or pyramidal shaped. At 6 months of age, there appear to be some dead motor neurons in both WT and GFAP/TDP-43 Δ NLS spinal cord. Fluorescent staining of GFAP in the spinal cord was minimal in white matter. The grey matter of the spinal cord showed an increase of TDP-43 which would be expected as normal distribution in nuclei but TDP-43 staining was punctate and suggests nuclear clearance and cytoplasmic accumulation. Astrocytic TDP-43 staining was not very clear to define astrocyte morphology in grey matter, but we assumed these astrocytes to be protoplasmic due to patterns of branching (Figure 8B).

Defined branching of TDP-43 positive astrocytes are seen in the dentate gyrus of GFAP/TDP-43 Δ NLS, which may account for behavior differences along with the alternative gene splicing data. We observed significant behavior changes in both spatial memory (short term memory), working memory and exploratory behavior (Figure 4 and Figure 5). Behavior of GFAP/TDP-43 Δ NLS mice was not representative of TDP-43WT mice (Alfieri et al., 2016). GFAP/TDP-43 Δ NLS mice were active and seemed to spend time exploring but were not enthused to explore the novel arm. Our model explored the whole y-maze like it was novel. Astrocytes function in the tripartite synapse and aid in synaptic transmission as well as glutamate uptake. These processes occur through connexin hemichannel and pannexin channels (Orellana et al., 2016). Our exon array data shows no splicing activity that directly affects connexins or pannexins, but ATP, calcium binding molecules and other complex and coded metabolic role

players are affected via splicing (Appendix B). NMDA and NMDARs are heavily involved in memory retention (Foley et al., 2008; Place et al., 2012; Tarabeux et al., 2011). Our model shows that several forms of NMDA (GRIN1, GRIN3a, and Nsmf as well as others) are spliced by astrocytic TDP-43 Δ NLS, therefore a reduction in memory makes sense. Reelin is a glycoprotein that is essential in development as well synaptic function. A direct correlation between Reelin and cognition and memory have been established. When reelin is reduced, LTP and memory is also reduced (Folsom & Fatemi, 2013). In this model, TDP-43 splices Reelin, therefore the normal function and efficiency of this protein is altered. Overall, seeing a change in memory with a small sample size and noticeable changes in the hippocampus such as astrocyte expression and myelin changes was significant.

Myelination occurs by oligodendrocytes establishing a myelin sheath around axons. Demyelination is a hallmark of neurodegeneration but may be repaired by remyelination if the cause of demyelination is not severe. Astrocytes are responsible for myelin maintenance via connexins. Astrocytes promote factors such as gamma-secretase and insulin-like growth factor I to support remyelination. While myelin basic protein itself isn't spliced by TDP-43 in this model, myelin basic protein repressor factor is spliced. This should allow remyelination of myelin basic protein but instead myelin basic protein is decreased in an age dependent manner (Figure 9). Myelination is promoted by many pathways such as the Akt-1 pathway, calcineurin-NFAT signaling pathway and Notch (Domingues et al., 2016; Gaesser & Fyffe-maricich, 2016; Lanciotti et al., 2013). Notch signaling contributes to development of myelin. Notch1 is only found in oligodendrocytes and in our model, hairless (which plays a role in notch signaling) is alternatively spliced. Semaphorins are also alternatively spliced. Semaphorins function in

axonal guidance during myelin formation but they also function in repression of myelination by promoting collapse of myelin (Taveggia, Feltri, & Wrabetz, 2011).

Alternative splicing activity of TDP-43 Δ NLS has contributed to non-cell autonomous effects in neurons and oligodendrocytes. Our model can be viewed from a neurodevelopment standpoint because TDP-43 Δ NLS was turned on during development. It can also be viewed from a neurodegenerative standpoint because our model displays age-dependent changes *in vivo*. Future studies include exploring myelination and memory pathways in depth to accurately identify mechanisms these age dependent changes. We also plan to verify alternative splice variants of GFAP as well as other genes of interest which include calcium binding genes. We would also like to characterize the GFAP/TDP-43 Δ NLS model while TDP-43 Δ NLS is turned off during development.

References

- Adamsky, A., & Goshen, I. (2017). Astrocytes in memory function: Pioneering findings and future directions. *Neuroscience*, (June). <http://doi.org/10.1016/j.neuroscience.2017.05.033>
- Alfieri, J. A., Silva, P. R., & Igaz, L. M. (2016). Early cognitive/social deficits and late motor phenotype in conditional wild-type TDP-43 transgenic mice. *Frontiers in Aging Neuroscience*, 8(DEC), 1–14. <http://doi.org/10.3389/fnagi.2016.00310>
- Ayala, Y. M., Conti, L. De, Dhir, A., Romano, M., Ambrogio, A. D., Tollervey, J., ... Baralle, F. E. (2011). TDP-43 regulates its mRNA levels through a negative feedback loop, *30*(2), 277–288. <http://doi.org/10.1038/emboj.2010.310>
- Ayala, Y. M., Zago, P., D'Ambrogio, A., Xu, Y.-F., Petrucelli, L., Buratti, E., & Baralle, F. E. (2008). Structural determinants of the cellular localization and shuttling of TDP-43. *Journal of Cell Science*, 121(22), 3778–3785. <http://doi.org/10.1242/jcs.038950>
- Ben Haim, L., Carrillo-de Sauvage, M.-A., Ceyzeriat, K., & Escartin, C. (2015). Elusive roles for reactive astrocytes in neurodegenerative diseases. *Frontiers in Cellular Neuroscience*, 9(August), 1–27. <http://doi.org/10.3389/fncel.2015.00278>
- Blitterswijk, M. Van, Baker, M. C., Bieniek, K. F., David, S., Josephs, K. A., Boeve, B., ... Rademakers, R. (2014). Profilin-1 mutations are rare in patients with amyotrophic lateral sclerosis and frontotemporal dementia, (1), 1–12. <http://doi.org/10.3109/21678421.2013.787630>. Profilin-1
- Buratti, E., Baralle, F. E., Buratti, E., & Baralle, F. E. (2017). processing and gene expression regulation The multiple roles of TDP-43 in pre-mRNA processing and gene expression regulation, *6286*(July). <http://doi.org/10.4161/rna.7.4.12205>

- Bushong, E. A., Martone, M. E., & Ellisman, M. H. (2004). Maturation of astrocyte morphology and the establishment of astrocyte domains during postnatal hippocampal development. *International Journal of Developmental Neuroscience*, 22(2), 73–86.
<http://doi.org/10.1016/j.ijdevneu.2003.12.008>
- Chandrasekaran, A., Avci, H. X., Leist, M., Kobolák, J., & Dinnyés, A. (2016). Astrocyte Differentiation of Human Pluripotent Stem Cells_ : New Tools for Neurological Disorder Research. *Frontiers in Cellular Neuroscience*, 10(September).
<http://doi.org/10.3389/fncel.2016.00215>
- Choi, M., Ahn, S., Yang, E.-J., Kim, H., Chong, Y. H., & Kim, H.-S. (2016). Hippocampus-based contextual memory alters the morphological characteristics of astrocytes in the dentate gyrus. *Molecular Brain*, 9(1), 72. <http://doi.org/10.1186/s13041-016-0253-z>
- Chvátal, A., Anderová, M., Neprasová, H., Prajerová, I., Benesová, J., Butenko, O., & Verkhatsky, A. (2008). Pathological potential of astroglia. *Physiological Research / Academia Scientiarum Bohemoslovaca*, 57 Suppl 3(Tower 1992).
- Cohen, T. J., Lee, V. M. Y., & Trojanowski, J. Q. (2012). TDP-43 functions and pathogenic mechanisms implicated in TDP-43 proteinopathies *Todd*, 17(11), 659–667.
<http://doi.org/10.1016/j.molmed.2011.06.004.TDP-43>
- Cykowski, M. D., Takei, H., Van Eldik, L. J., Schmitt, F. A., Jicha, G. A., Powell, S. Z., & Nelson, P. T. (2016). Hippocampal sclerosis but not normal aging or Alzheimer disease is associated with TDP-43 pathology in the basal forebrain of aged persons. *Journal of Neuropathology and Experimental Neurology*, 75(5), 397–407.

<http://doi.org/10.1093/jnen/nlw014>

- De Keyser, J., Mostert, J. P., & Koch, M. W. (2008). Dysfunctional astrocytes as key players in the pathogenesis of central nervous system disorders. *Journal of the Neurological Sciences*, 267(1–2), 3–16. <http://doi.org/10.1016/j.jns.2007.08.044>
- Domingues, H. S., Portugal, C. C., Socodato, R., & Relvas, J. B. (2016). Oligodendrocyte, Astrocyte and Microglia Crosstalk in Myelin Development, Damage, and Repair. *Frontiers in Cell and Developmental Biology*, 4, 1–16. <http://doi.org/10.3389/fcell.2016.00079>
- Emsley, J. G., & Macklis, J. D. (2007). Astroglial heterogeneity closely reflects the neuronal-defined anatomy of the adult murine CNS. *Neuron Glia Biology*, 2(3), 175–186.
- Estes, P. S., Daniel, S. G., Mccallum, A. P., Boehringer, A. V, Sukhina, A. S., & Rebecca, A. (2013). Motor neurons and glia exhibit specific individualized responses to TDP-43 expression in a Drosophila model of amyotrophic lateral sclerosis, 6(3), 721–733. <http://doi.org/10.1242/dmm.010710>
- Foley, N. H., Bray, I., Watters, K. M., Das, S., Bernas, T., Prehn, J. H. M., & Stallings, R. L. (2008). Memory in Caenorhabditis elegans is Mediated By NMDA-Type Ionotropic Glutamate Receptors Takashi. *Current Biology*, 18(13), 1089–1098. <http://doi.org/10.1038/cdd.2010.172>.MicroRNAs
- Folsom, T. D., & Fatemi, S. H. (2013). The Involvement of Reelin in Neurodevelopmental Disorders. *Neuropharmacology*, (68), 2166–2171. <http://doi.org/10.1021/nl061786n>.Core-Shell
- Gaesser, J. M., & Fyffe-maricich, S. L. (2016). Intracellular signaling pathway regulation of myelination and remyelination in the CNS. *Experimental Neurology*, 283, 501–511.

<http://doi.org/10.1016/j.expneurol.2016.03.008>

Gendron, T.F.; Josephs, K.A.; Petrucelli, L. (2011). Transactive response DNA-binding protein 43 (TDP-43): mechanisms of neurodegeneration, *36*(2), 97–112.

<http://doi.org/10.1111/j.1365-2990.2010.01060.x>.Review

Hayakawa, K., Esposito, E., Wang, X., Terasaki, Y., Liu, Y., Xing, C., ... Hospital, X. (2017). Transfer of mitochondria from astrocytes to neurons after stroke, *535*(7613), 551–555.

<http://doi.org/10.1038/nature18928>.Transfer

Heaven, M. R., Flint, D., Randall, S. M., Sosunov, A. A., Wilson, L., Barnes, S., ... Brenner, M. (2016). Composition of Rosenthal Fibers, the Protein Aggregate Hallmark of Alexander Disease. *Journal of Proteome Research*, *15*(7), 2265–2282.

<http://doi.org/10.1021/acs.jproteome.6b00316>

Henneberger, C., Papouin, T., Oliet, S. H. R., & Rusakov, D. A. (2010). Long-term potentiation depends on release of d-serine from astrocytes. *Nature*, *463*(7278), 232–236.

<http://doi.org/10.1038/nature08673>

Huang, C. (2015). Profiling the Genes Affected by Pathogenic TDP-43 in Astrocytes, *129*(6), 932–939. <http://doi.org/10.1111/jnc.12660>.Profiling

Huang, C., Huang, B., Bi, F., Yan, L. H., Tong, J., Huang, J., ... Zhou, H. (2014). Profiling the genes affected by pathogenic TDP-43 in astrocytes. *Journal of Neurochemistry*, *129*(6), 932–939. <http://doi.org/10.1111/jnc.12660>

<http://doi.org/10.1111/jnc.12660>

Lanciotti, A., Brignone, M. S., Bertini, E., Petrucci, T. C., Aloisi, F., Ambrosini, E., ... Elena, V. R. (2013). ASTROCYTES_: EMERGING STARS IN LEUKODYSTROPHY PATHOGENESIS, *4*(2), 1–37. <http://doi.org/10.2478/s13380-013-0118-1>.ASTROCYTES

- Liu, Y., Chiang, P., & Tsai, K. (2013). Disease Animal Models of TDP-43 Proteinopathy and Their Pre-Clinical Applications, 20079–20111. <http://doi.org/10.3390/ijms141020079>
- Liu, Y., Wang, L., Long, Z., Zeng, L., & Wu, Y. (2012). Protoplasmic Astrocytes Enhance the Ability of Neural Stem Cells to Differentiate into Neurons In Vitro, 7(5).
<http://doi.org/10.1371/journal.pone.0038243>
- Magavi, S., Friedmann, D., Banks, G., Stolfi, A., & Lois, C. (2012). Coincident generation of pyramidal neurons and protoplasmic astrocytes in neocortical columns. *The Journal of Neuroscience*: *The Official Journal of the Society for Neuroscience*, 32(14), 4762–72.
<http://doi.org/10.1523/JNEUROSCI.3560-11.2012>
- Molofsky, A. V., Krennick, R., Ullian, E., Tsai, H. H., Deneen, B., Richardson, W. D., ... Rowitch, D. H. (2012). Astrocytes and disease: A neurodevelopmental perspective. *Genes and Development*, 26(9), 891–907. <http://doi.org/10.1101/gad.188326.112>
- Newman, L. A., Korol, D. L., & Gold, P. E. (2011). Lactate produced by glycogenolysis in astrocytes regulates memory processing. *PLoS ONE*, 6(12).
<http://doi.org/10.1371/journal.pone.0028427>
- Oberheim, N. A., Goldman, S. A., & Nedergaard, M. (2012). Heterogeneity of Astrocytic Form and Function. *Methods in Molecular Biology*, 814, 23–45. <http://doi.org/10.1007/978-1-61779-452-0>
- Olabarria, M., Putilina, M., Riemer, E. C., & Goldman, J. E. (2015). Astrocyte pathology in Alexander disease causes a marked inflammatory environment. *Acta Neuropathologica*, 130(4), 469–486. <http://doi.org/10.1007/s00401-015-1469-1>
- Orellana, J. A., Retamal, M. A., Moraga-Amaro, R., & Stehberg, J. (2016). Role of Astroglial

- Hemichannels and Pannexons in Memory and Neurodegenerative Diseases. *Frontiers in Integrative Neuroscience*, 10(July), 1–9. <http://doi.org/10.3389/fnint.2016.00026>
- Perng, M. Der, Su, M., Wen, S. F., Li, R., Gibbon, T., Prescott, A. R., ... Quinlan, R. A. (2006). The Alexander Disease–Causing Glial Fibrillary Acidic Protein Mutant, R416W, Accumulates into Rosenthal Fibers by a Pathway That Involves Filament Aggregation and the Association of α -B-Crystallin and HSP27. *The American Journal of Human Genetics*, 79(2), 197–213. <http://doi.org/10.1086/504411>
- Place, R., Lykken, C., Beer, Z., Suh, J., McHugh, T. J., Tonegawa, S., ... Sauvage, M. M. (2012). NMDA signaling in CA1 mediates selectively the spatial component of episodic memory. *Learning & Memory*, 19(4), 164–169. <http://doi.org/10.1101/lm.025254.111>
- Serio, A., Bilican, B., Barmada, S. J., Ando, D. M., Zhao, C., Siller, R., ... Chandran, S. (2013). Astrocyte pathology and the absence of non-cell autonomy in an induced pluripotent stem cell model of TDP-43 proteinopathy. *Proceedings of the National Academy of Sciences*, 110(12), 4697–4702. <http://doi.org/10.1073/pnas.1300398110>
- Serio, A., Bilican, B., Barmada, S. J., Michael, D., Zhao, C., Siller, R., & Burr, K. (2013). Astrocyte pathology and the absence of non-cell autonomy in an induced pluripotent stem cell model of TDP-43 proteinopathy, 110(12). <http://doi.org/10.1073/pnas.1300398110>
- Sofroniew, M. V., & Vinters, H. V. (2010). Astrocytes: biology and pathology, 7–35. <http://doi.org/10.1007/s00401-009-0619-8>
- Stahnisch, F. W., & Bulloch, A. G. M. (2011). Mihaly (Michael von) Lenhossek (1863–1937), 1901–1903. <http://doi.org/10.1007/s00415-011-6035-8>
- Stork, T., Sheehan, A., Tasdemir-yilmaz, O. E., & Freeman, M. R. (2015). Neuron-glia

interactions through the Heartless FGF receptor signaling pathway mediate morphogenesis of *Drosophila* astrocytes. *Neuron*, 83(2), 388–403.

<http://doi.org/10.1016/j.neuron.2014.06.026>.Neuron-glia

Tarabeux, J., Kebir, O., Gauthier, J., Hamdan, F. F., Xiong, L., Piton, A., ... Krebs, M.-O.

(2011). Rare mutations in N-methyl-D-aspartate glutamate receptors in autism spectrum disorders and schizophrenia. *Translational Psychiatry*, 1(11), e55.

<http://doi.org/10.1038/tp.2011.52>

Taveggia, C., Feltri, M. L., & Wrabetz, L. (2011). Signals to promote myelin formation and repair, 6(January 2010), 276–287. <http://doi.org/10.1038/nrneurol.2010.37>.Signals

Thermofisher. (n.d.). Identifying and Validating Alternative Splicing Events, 2685.

Tollervey, J. R., Curk, T., Rogelj, B., Briese, M., & Cereda, M. (2011). Characterising the RNA targets and position-dependent splicing regulation by TDP-43; implications for neurodegenerative diseases. *October*, 14(4), 452–458.

<http://doi.org/10.1038/nn.2778>.Characterising

Tsao, W., Jeong, Y. H., Lin, S., Ling, J., Price, D. L., Chiang, P. M., & Wong, P. C. (2012).

Rodent models of TDP-43: Recent advances. *Brain Research*, 1462, 26–39.

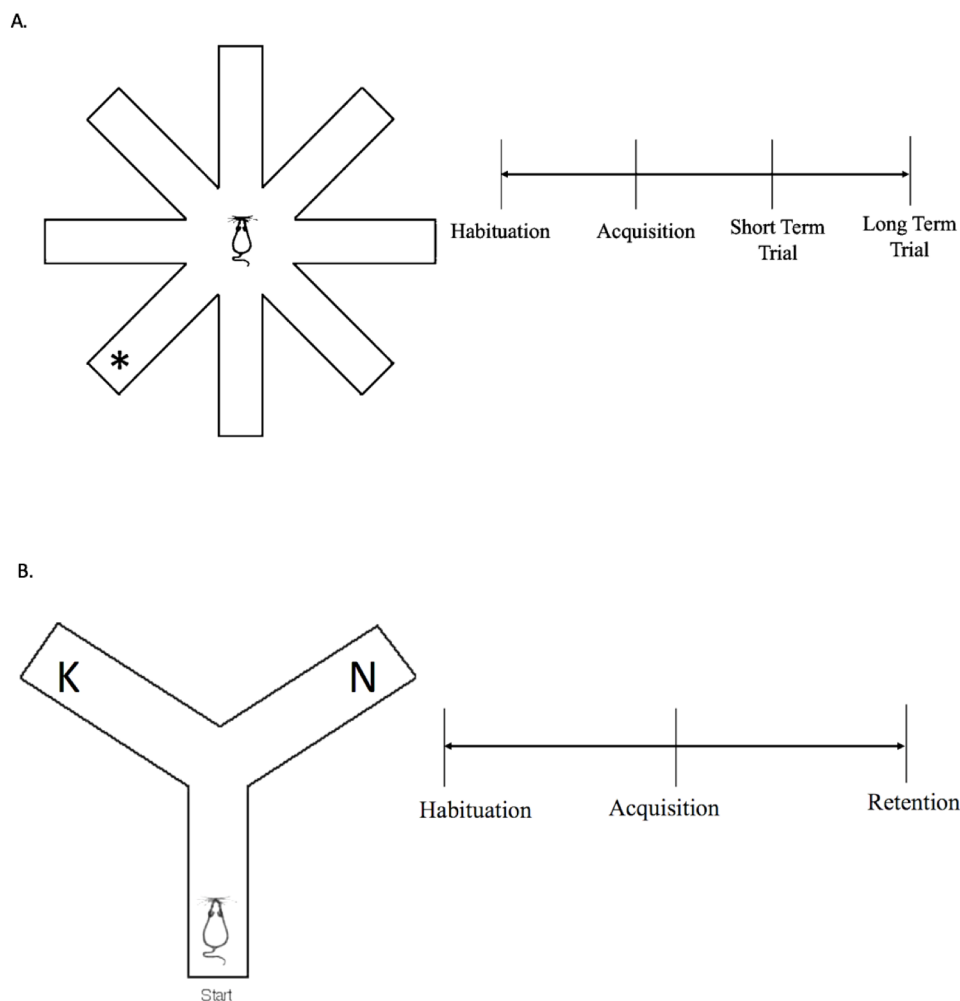
<http://doi.org/10.1016/j.brainres.2012.04.031>

Vasile, F., Dossi, E., & Rouach, N. (2017). Human astrocytes: structure and functions in the healthy brain. *Brain Structure and Function*, 0(0), 0. <http://doi.org/10.1007/s00429-017-1383-5>

Verkhatsky, A., Matteoli, M., Parpura, V., Mothet, J.-P., & Zorec, R. (2016). Astrocytes as secretory cells of the central nervous system: idiosyncrasies of vesicular secretion. *The*

- EMBO Journal*, 35(3), 239–257. <http://doi.org/10.15252/embj.201592705>
- Walker, A. K., Daniels, C. M. L., Goldman, J. E., Trojanowski, J. Q., Lee, V. M.-Y., & Messing, A. (2014). Astrocytic TDP-43 Pathology in Alexander Disease. *Journal of Neuroscience*, 34(19), 6448–6458. <http://doi.org/10.1523/JNEUROSCI.0248-14.2014>
- Wilhelmsson, U. (2004). Absence of Glial Fibrillary Acidic Protein and Vimentin Prevents Hypertrophy of Astrocytic Processes and Improves Post-Traumatic Regeneration. *Journal of Neuroscience*, 24(21), 5016–5021. <http://doi.org/10.1523/JNEUROSCI.0820-04.2004>
- Winton, M. J., Igaz, L. M., Wong, M. M., Kwong, L. K., Trojanowski, J. Q., & Lee, V. M. Y. (2008). Disturbance of nuclear and cytoplasmic TAR DNA-binding protein (TDP-43) induces disease-like redistribution, sequestration, and aggregate formation. *Journal of Biological Chemistry*, 283(19), 13302–13309. <http://doi.org/10.1074/jbc.M800342200>
- Wobst, H. J., Delsing, L., Brandon, N. J., & Moss, S. J. (2017). Truncation of the TAR DNA-binding protein 43 is not a prerequisite for cytoplasmic relocalization, and is suppressed by caspase inhibition and by introduction of the A90V sequence variant. *Plos One*, 12(5), e0177181. <http://doi.org/10.1371/journal.pone.0177181>
- Yang, C., Wang, H., Qiao, T., Yang, B., Aliaga, L., Qiu, L., ... Xu, Z. (2014). Partial loss of TDP-43 function causes phenotypes of amyotrophic lateral sclerosis. *Proceedings of the National Academy of Sciences of the United States of America*, 111(12), E1121-9. <http://doi.org/10.1073/pnas.1322641111>
- Zhang, X., Zhang, J., & Chen, C. (2009). Long-Term Potentiation at Hippocampal Perforant Path-Dentate Astrocyte Synapses. *Biochem Biophys Res Commun*, 23(1), 1–7. <http://doi.org/10.1038/jid.2014.371>

Appendix A



Schematic of apparatus used for behavior studies

(A) Radial Arm Maze. "*" denotes baited arm for mice. Mice were food deprived for 16 hours prior to habituation. Timeline includes acquisition trial of 15 minutes which allowed mice to explore maze and all mice were able to find bait in this trial. Short term trial was performed an hour later and mice were allotted 5 minutes to explore the maze. Mice were again food deprived for 16 hours prior to a second habituation. Then memory was tested again in the long term trial where mice were allotted 5 minutes in the maze.

(B) Y-maze. "K" denotes known arm and "N" denotes novel arm. Mice were habituated in the testing room. For the acquisition phase, the novel arm was blocked by a piece of sheet metal and mice were allowed to explore the known arm for 10 minutes. For the retention trial, mice were exposed to the known and novel arm and activity was tracked for 5 minutes.

Appendix B

Gene Fold Change	Gene Symbol	Cellular Localization	Function	Group	Splicing Index (Control vs. NLS)	ANOVA p-value (Control vs. NLS)
3.48	Hsd11b1	endoplasmic reticulum membrane	catalyzes reversible conversion of cortisol to inactive metabolite cortisol	Complex	-2.02	0.001613
2.94				NonCoding	-1.71	0.042871
2.09	RP23-103112.3			NonCoding	-1.78	0.023511
2	Agxt2l1	mitochondrion	catalyzes conversion to ammonia, inorganic phosphate and acetaldehyde	Complex	-1.58	0.010154
1.95				NonCoding	-1.77	0.030198
1.94	Fam150b	extracellular - secretion	Ligand of LTK and ALK, possibly responsible for cell proliferation	Coding	-2.25	0.010532
1.89	Sfrp5	extracellular - secretion	modulator of WNT signaling, regulation of cell growth and differentiation	Coding	-1.48	0.017113
1.88	Gm6818			Coding	-1.5	0.03184
1.88				NonCoding	-1.75	0.047806
1.86				NonCoding	-1.2	0.038205
1.85	Dao	peroxisome	regulates neuromodulator D-serine	Complex	-1.52	0.003624
1.85				NonCoding	-1.68	0.026027
1.8				NonCoding	-1.7	0.017822
1.78	Stab1	membrane	scavenger receptor and may defend bacterial infections	Complex	-1.6	0.027057
1.76				NonCoding	-2.12	0.004326
1.76				NonCoding	-1.77	0.007655
1.75	Gm11149			Complex	-1.33	0.01625
1.73				NonCoding	-1.93	0.047391
1.72				NonCoding	1.29	0.015405
1.71	Gja1	cell membrane, gap junction, endoplasmic reticulum	regulates bladder capacity	Complex	-1.92	0.010173
1.7	Vstm4	secreted - cell membrane	enhances voltage gated calcium channel in retinal photoreceptors	Coding	-1.84	0.009402
1.7	Gvin1	cytoplasm, nucleus	GTP binding	Coding	-1.57	0.00691
1.69	Nsat1700084C01Rik	cytoplasm	involved in development	Complex	-1.74	0.0244
1.67				Coding	1.19	0.020071
1.65				NonCoding	-1.18	0.000091
1.65				NonCoding	-1.73	0.019917
1.64	Calr4	endoplasmic reticulum	calcium binding site	Complex	-1.28	0.021068
1.63	Gm3912		nucleic acid binding	Complex	-1.61	0.01254
1.62	Hmgcs2D230002A01Rik	mitochondrion	catalysis and condensation	Coding	1.09	0.038787
1.61				NonCoding	-1.32	0.028025
1.61	Slc1a3			Complex	-1.21	0.03945
1.59	Xlr3b	membrane	transportation and termination of postsynaptic glutamate action	Complex	1.28	0.018751
1.57				NonCoding	-2	0.027321
1.56				NonCoding	-1.73	0.012073
1.55	mmu-mir-63904930524B15Rik			NonCoding	-1.8	0.013817
1.54				Coding	-1.73	0.004011
1.54	Dmp1	nucleus, cytoplasm, secreted	calcium ion, extracellular matrix and integrin binding	Coding	-1.43	0.040101
1.54	Duxbl2	nucleus	DNA binding	Complex	-1.24	0.020361
1.53	Serpine2	secreted	inhibitor, promotes neurite extension	Complex	-1.74	0.043195
1.53				NonCoding	-1.86	0.008908
1.53	Gm26611			NonCoding	-1.57	0.021318
1.52	Acss1	mitochondrion matrix	energy homeostasis	Complex	-1.05	0.032244
1.51				NonCoding	1.06	0.04701
1.5				NonCoding	-1.75	0.00589
1.5	1700095B22Rik			NonCoding	-1.66	0.038013
1.49	Fam227b			Complex	-1.42	0.04152
1.49				NonCoding	-1.56	0.001864
1.49	Lhfpl1	membrane		Coding	-1.49	0.003715
1.49	Trp631700088E04Rik	nucleus	DNA binding transcriptional activator or repressor	Complex	-1.55	0.004748
1.48				Complex	-1.33	0.014233
1.48	Gm68211700007F19Rik			Coding	1.14	0.046842
1.48				NonCoding	-1.45	0.047134
1.47	Gpr98	membrane	calcium binding and role in development	Complex	-1.38	0.034663
1.47	Mpeg1	membrane	macrophage	Coding	-1.29	0.026556
1.46	Sfxn5	mitochondrion membrane	citrate transporter	Complex	-1.37	0.025699
1.46	Gm5929			Complex	-1.14	0.007903

Appendix B. TDP-43 Alternative Gene splicing in GFAP/TDP-43ΔNLS model

Only gene fold change ≤ 1.25 is shown but all data from exon array was used in this study

1.46	Olfir59	membrane	GPCR and olfactory receptor activity	Coding	-1.34	0.035679
1.46	Ppww1	nucleus	accelerate the folding of proteins and mRNA splicing via spliceosome	Complex	-1.41	0.035721
1.45	Mif1	nucleus and cytoplasm	DNA binding and cell cycle arrest	Complex	-2.35	0.034103
1.44	Olfir287	membrane	GPCR and olfactory receptor activity	Complex	-1.12	0.02335
1.44	Paps2	cytosol	sulfate assimilation	Complex	-1.42	0.036344
1.44				NonCoding	-1.74	0.009355
1.44	Pipox	peroxisome	metabolism of sarcosine, L-pipecolic acid and L-proline	Complex	1.2	0.016385
1.44				NonCoding	-1.31	0.017135
1.43				NonCoding	-1.36	0.025582
1.43				NonCoding	-1.48	0.004943
1.43				NonCoding	-1.07	0.012053
1.42				NonCoding	-1.39	0.000106
1.42	Paqr6	membrane	steroid binding and steroid hormone receptor activity	Complex	-1.47	0.002495
1.42				NonCoding	-1.74	0.02469
1.42	Xlr3a	nucleus	spermatid development	Complex	1.35	0.012584
1.42	Pmch	secreted	neurotransmitter or neuromodulator	Coding	-1.66	0.037223
1.42	BB218582			NonCoding	-2.89	0.041234
1.41	Erv3	extracellular exosome	mediation of receptor recognition and membrane fusion during early infection	Coding	-1.59	0.000134
1.41	Ak4	mitochondrion matrix	catalysis of interconversion of nucleoside phosphates	Complex	-1.53	0.016021
1.41	Dcaf1211			Coding	-1.08	0.047583
1.41	Gpd1		catalytic activity	Complex	-1.37	0.003329
1.41	Tas2r108	cilium membrane	receptor	Coding	-1.24	0.003987
1.41	Ngef	cytoplasm, membrane and axonal growth cone	regulation of signaling pathways and GTPase activity	Complex	1.23	0.02946
1.41	Fam169b			Complex	-1.27	0.039417
1.41	Olfir153	cell membrane	GPCR and olfactory receptor activity	Coding	-1.55	0.016502
1.41	Niacr1	cell membrane	nicotinic acid receptor activity, purinergic nucleotide receptor activity, GTP binding	Coding	-1.28	0.019984
1.41				NonCoding	-1.35	0.039978
1.41	5430427O19Rik			Coding	1.09	0.035199
1.41				NonCoding	-1.18	0.046174
1.4	Gm19866			NonCoding	-1.56	0.000324
1.4	Acaa2	mitochondrion	lipid metabolism	Coding	1.17	0.015045
1.4	Lbp	secreted	lipid binding	Complex	-1.19	0.045094
1.4	Ccdc33			Complex	-1.76	0.033092
1.4	Gm6994			Complex	-1.27	0.041182
1.4				NonCoding	-1.75	0.046557
1.39	Zrsr2	nucleus	pre-mRNA 3' splice site binding	Complex	-1.23	0.004347
1.39				NonCoding	-1.97	0.001346
1.39	4930548J01Rik			NonCoding	1.16	0.025562
1.39	Dnm3os		skeletal system development	Complex	-1.54	0.013386
1.39	Aeadl	mitochondrion matrix	FAD binding and metabolic activity	Complex	-1.26	0.027468
1.39	Gm10538			NonCoding	-1.5	0.017344
1.39	Ndr2	cytoplasm and axonal growth cone	cell differentiation and Wnt signaling pathway	Coding	-1.17	0.019429
1.39	D730001G18Rik			Complex	-1.46	0.020323
1.39	Zbbx	intracellular	zinc ion binding	Coding	1.94	0.031366
1.39	Rp1	cytoplasm	microtubule binding	Complex	-1.51	0.042972
1.39	Fabp7	cytoplasm	lipid binding and transporter activity	Coding	-1.12	0.047686
1.38	Lthp1	secreted	calcium ion binding and transforming growth factor binding	Complex	-1.4	0.025595
1.38				NonCoding	-1.32	0.003121
1.38	Rgs22	cytoplasm and nucleus	GTPase activator activity	Complex	1.1	0.013456
1.38	Gm6592	nucleus	nucleic acid binding	Coding	-1.25	0.014619
1.38	Olfir631	cell membrane	GPCR and olfactory receptor activity	Coding	-1.35	0.020367
1.38				NonCoding	-1.53	0.021041
1.38	Epas1	nucleus	DNA binding and transcription factor binding	Complex	-1.08	0.0367
1.38				NonCoding	-1.26	0.02734
1.38				NonCoding	1.09	0.03929
1.38				NonCoding	-1.85	0.039415
1.37	Dnaic1	cytoplasm	motor activity	Complex	1.3	0.010342
1.37	Asrg11	cytoplasm	metabolic activity	Complex	-1.24	0.010662
1.37	Hhat1	secreted	intercellular signaling for development	Complex	1.13	0.021294

Appendix B (Continued)

1.37				NonCoding	-1.23	0.041049
1.37	Hdde3		involved in starvation response	Coding	-1.11	0.010339
1.37				NonCoding	-1.4	0.032322
1.37	Nwd1	cytoplasm, nucleus, cell membrane and secreted	cell cycle control and signal transduction	Complex	-1.3	0.021681
1.37	Gm872			Complex	-1.37	0.034796
1.37	Gm12970			NonCoding	-1.97	0.026953
1.37				NonCoding	-1.35	0.03079
1.37	Maats1	cytoplasm and mitochondrion	cilium movement	Complex	-1.24	0.042247
1.37	Tnni1	cytosol and troponin complex	actin binding	Complex	-1.7	0.044386
1.37	Lin28a	cytoplasm, rough endoplasmic reticulum, nucleus and nucleolus	DNA binding, miRNA binding, mRNA binding and RNA binding	Coding	-1.72	0.047906
1.36	Gm14015			NonCoding	-1.2	0.000216
1.36	2900052N01Rik			NonCoding	-1.51	0.015434
1.36	Myo10	cytoplasm	actin filament binding, ATP binding, calmodulin binding and motor activity	Complex	-1.37	0.011791
1.36	Rspb9	cytoplasm	component of axonemal radial spoke head	Complex	-1.4	0.0075
1.36	Gm20580			Coding	-1.36	0.025661
1.36	Gm16083			NonCoding	-1.22	0.015224
1.36	Spag17	cytoplasm	plays a role in function and structure motile cilia	Complex	-1.11	0.040826
1.36	Gm20997			Complex	-1.64	0.027202
1.36	1700109G14Rik			NonCoding	1.41	0.033766
1.36				NonCoding	-1.4	0.046682
1.36	RP23-230F2.8			NonCoding	-1.25	0.049132
1.35				NonCoding	-1.68	0.028968
1.35	Gm2022			Complex	-1.49	0.003138
1.35	Gm4070			Complex	-1.28	0.003608
1.35	Pi15	secreted	peptidase inhibitor activity	Coding	1.31	0.042768
1.35	2610034M16Rik			Complex	-1.32	0.015398
1.35	Sulfl	endoplasmic reticulum, golgi apparatus and cell surface	facilitates apoptosis	Complex	-1.34	0.025572
1.35				NonCoding	-1.96	0.024498
1.35	Gm15055			NonCoding	-1.62	0.030067
1.35				NonCoding	-1.13	0.038023
1.35	Gm11578			Pseudogene	-1.68	0.039588
1.35				NonCoding	1.48	0.046454
1.35	Cd38	membrane	synthesis of second messenger	Coding	1.16	0.049608
1.34	Arhge26	cytosol	promotion of exchange of GDP by GTP	Complex	-1.33	0.000406
1.34	Prex2	cytoplasm and plasma membrane	activates Rac proteins by exchanging bound GDP for free GTP	Complex	-1.25	0.027461
1.34	Mfap5	secreted	plays a role in hematopoiesis	Complex	-1.21	0.007849
1.34				NonCoding	-1.68	0.008343
1.34	Dnah12		force generating protein	Coding	-1.31	0.010185
1.34	Tom111	cytoplasm golgi apparatus, endosome membrane and membrane	adapter protein involved in signaling proteins	Complex	-1.04	0.04841
1.34				NonCoding	-1.26	0.016636
1.34	BC037032			NonCoding	-1.21	0.049234
1.34	Lum	extracellular exosome	collagen binding	Coding	-1.3	0.019817
1.34				Complex	-1.6	0.041341
1.34	5730457N03Rik			NonCoding	-1.22	0.024752
1.34	Tex12	nucleoplasm	DNA synthesis repair	Coding	-1.41	0.029256
1.34	Zfp419			Complex	-1.39	0.029432
1.34	Smlr1	membrane		Complex	-1.16	0.043632
1.34	Smlr1			Complex	-1.42	0.032499
1.34	1700012B09Rik			Complex	-1.51	0.032612
1.34				NonCoding	-1.67	0.043069
1.33	Prtg	membrane	plays a role in anteroposterior axis elongation	Complex	-1.36	0.000623
1.33	Serhl	cytoplasm and peroxisome	enzymatic functions related to cell muscle hypertrophy	Complex	1.6	0.016019
1.33	Lix1	cytoplasm	autophagosome maturation	Complex	-1.6	0.030249
1.33	Col12a1	secreted	cell adhesion and fibril organization	Complex	-1.38	0.029934
1.33	D930020B18Rik			Coding	-1.45	0.016921

Appendix B (Continued)

1.33	Setd7	cytoplasm, nucleus, endoplasmic reticulum and mitochondrion matrix	induction of growth arrest or apoptosis	Complex	-1.36	0.00531
1.33				NonCoding	-1.43	0.040112
1.33	Nsun2	nucleus and cytoplasm	methylates tRNA	NonCoding	-1.22	0.007851
1.33	Phkg1	cytosol	mediates breakdown of neural and hormonal glycogen	Complex	-1.48	0.01068
1.33	Vmn1r172		pheromone receptor activity	Coding	-1.57	0.012872
1.33	Dnajb13	cilium and flagellum	unfolded protein binding	Complex	1.18	0.038344
1.33	Cyp4f41-ps			Complex	-1.66	0.020841
1.33	Man2e1 4930448K2 ORik	cytosol, nucleoplasm and vacuole	carbohydrate binding	Complex	-1.7	0.022147
1.33				Complex	-1.3	0.032392
1.33	Slc14a1	cell membrane	urea and water transmembrane transporter activity	Complex	-1.27	0.033139
1.32	Slc15a2			Complex	-1.32	0.044258
1.32				NonCoding	-1.13	0.001877
1.32	1700125G0 2Rik			NonCoding	-1.23	0.002685
1.32	Lemd1	membrane		Complex	-1.42	0.005079
1.32	Slc22a4	membrane	antiporter activity	Complex	1.12	0.034918
1.32	Slc22a4			Complex	1.12	0.013116
1.32	Spag16	cytoplasm	protein kinase binding	Complex	-1.7	0.012033
1.32	Phka1	cell membrane	calmodulin binding and phosphorylase kinase activity	Complex	-1.07	0.032461
1.32	Rad51ap2	nucleus, cytoplasm, mitochondrion matrix and centrosome	DNA repair	Coding	-1.97	0.026399
1.32	Klhdc7a	membrane	protein ubiquitination	Complex	-1.66	0.026946
1.32				NonCoding	1.35	0.028903
1.31				NonCoding	-2.17	0.000676
1.31	Slc1a2	membrane	symporter and transmembrane activity	Complex	-1.24	0.011091
1.31	Dhx58	cytoplasm	ATP and DNA binding	Complex	-1.28	0.024839
1.31	Mettl7a3	membrane	methyltransferase activity	Coding	-1.28	0.0009
1.31				NonCoding	1.19	0.001358
1.31	Baalc	cytoplasm, synatosome and postsynaptic membrane	synaptic role through interaction with CAMK2A	Complex	-1.58	0.001665
1.31	Unc13a	cytoplasm and presynaptic membrane	vesicle maturation during exocytosis and neurotransmitter release	Complex	-1.64	0.034559
1.31				NonCoding	-1.58	0.005465
1.31	Tmem51	membrane	transmembrane protein	Coding	-1.1	0.006505
1.31	Acsf2	mitochondrion	catalysis of initial fatty acid metabolism	Complex	1.11	0.017408
1.31				NonCoding	-1.66	0.017528
1.31	Gm5397			Pseudogene	-1.09	0.022517
1.31	Fads2	endoplasmic reticulum membrane	involved in polyunsaturated fatty acid biosynthesis pathway	Coding	-1.12	0.023142
1.31	Rarres2	secreted	receptor binding	Complex	-1.19	0.043315
1.31	Pbdc1	cytoplasm	involved in polysaccharide biosynthesis	Complex	1.07	0.028402
1.31	Kcnj16	membrane	inward rectifier potassium channel	Coding	1.92	0.032044
1.31	D330050G 23Rik			NonCoding	-1.33	0.03327
1.31	Gm5176			Complex	-1.46	0.035892
1.31	Rnasel	cytoplasm and mitochondrion	RNA binding and rRNA binding	Complex	1.29	0.037845
1.31				NonCoding	-1.28	0.038143
1.31	Prrg4	membrane	calcium ion binding	Coding	-1.47	0.038688
1.3	2010015L0 4Rik			Complex	1.2	0.001419
1.3	Zfp618	nucleus	transcriptional regulation	Complex	-1.29	0.010913
1.3				NonCoding	-1.44	0.003771
1.3				NonCoding	1.35	0.004689
1.3	Trav4n-3			Complex	-1.5	0.041187
1.3	Gm6289			Coding	1.24	0.009639
1.3	Gm11387			Pseudogene	-1.27	0.046714
1.3	Hsd17b13	secreted	oxidoreductase activity	Complex	-1.17	0.049108
1.3				NonCoding	-1.73	0.016197
1.3	Lgi4	secreted	glial cell proliferation and neuron maturation	Complex	-1.31	0.016596
1.3	Rfx4	nucleus	transcriptional activator activity	Complex	-1.22	0.020091
1.3				NonCoding	-1.56	0.021212
1.3				NonCoding	-1.54	0.025278
1.3	Spf2		essential for axonemal development	Coding	-1.18	0.026493
1.3	Gm8016			Complex	-1.15	0.029515

Appendix B (Continued)

1.3				NonCoding	-1.13	0.03093
1.3	1700018A04Rik			NonCoding	-1.39	0.037222
1.3				NonCoding	-1.34	0.042123
1.3	Kcng1	cell membrane	delayed rectifier potassium channel activity	Coding	-1.49	0.044676
1.3	Ssxb8	intracellular	nucleic acid binding	Coding	-1.3	0.048633
1.29	Mrc1	membrane	regulates endocytosis by macrophage activity	Complex	-1.11	0.034709
1.29	Mdk	secreted	growth factor activity	Coding	-1.17	0.001158
1.29	Ldhc	cytoplasm	catalytic activity	Coding	-1.55	0.010027
1.29	Map3k19	cytoplasm	catalytic activity	Coding	-1.22	0.016541
1.29				NonCoding	-1.36	0.017887
1.29				NonCoding	-1.26	0.018589
1.29	Gm8540			Complex	-1.34	0.046311
1.28	Airn	nuclear chromosomes	regulates gene expression	NonCoding	-1.43	0.031273
1.28	Bear3	intracellular	regulation of proliferation in breast cancer cells and regulation of cellular adhesion	Coding	-1.32	0.001228
1.28	Bear3			Coding	1.26	0.00537
1.28	Copz2	cytoplasm	transport	Complex	-1.51	0.034338
1.28	Cpa1	secreted	proteolysis	Complex	-1.25	0.005721
1.28	Spata18	cytoplasm, mitochondrial outer membrane	regulation of mitochondrion quality	Coding	-1.26	0.037179
1.28	Nnt	mitochondrion inner membrane	metabolism and ROS detoxification	Complex	1.11	0.045838
1.28				NonCoding	-1.68	0.009476
1.28	Nme9	cytoplasm	regulation of microtubule function	Complex	-1.2	0.013703
1.28	Apedd1	cell membrane	Wnt signaling pathway and Wnt protein binding	Complex	-1.46	0.016579
1.28	Ccdc135	cytoplasm, cytoskeleton and motile cilium	regulation of flagellar motility	Coding	-1.22	0.018276
1.28	Wnt7a	secreted	frizzled binding, receptor binding	Complex	-1.22	0.018332
1.28	2310022B05Rik			Coding	1.07	0.020424
1.28	A630001G21Rik			Complex	-1.45	0.022251
1.28	A630001G21Rik			Complex	-1.25	0.043718
1.28	2810047C21Rik1			Complex	-1.18	0.039197
1.28	Vmn2r47	cell membrane	GPCR activity	Coding	-1.21	0.023827
1.28	S100a1	cytoplasm	calcium signal transducer	Coding	-1.1	0.024794
1.28	Tprg	synaptic vesicle membrane	identical protein binding	Complex	1.1	0.02862
1.28	Lpl	cell membrane, secreted	apolipoprotein binding	Complex	-1.32	0.04703
1.27	Atp1a2	membrane	ATP binding , catalytic activity	Complex	-1.18	0.005141
1.27				NonCoding	-1.33	0.034666
1.27	Hoxa9	nucleus	enzyme binding, transcriptional activator activity	Complex	-1.25	0.000792
1.27	Ceacam- ps1			Complex	-1.73	0.001032
1.27				NonCoding	-1.38	0.001823
1.27	Gpam	mitochondrion outer membrane	metabolic activity	Complex	1.14	0.003319
1.27	Lrrc34			Coding	-1.88	0.021007
1.27	P4ha3	endoplasmic reticulum lumen	iron ion binding	Complex	-1.12	0.007356
1.27	Traf1			Complex	-1.25	0.032954
1.27	Gm16386			NonCoding	-1.64	0.009082
1.27	4930572O13Rik			NonCoding	-1.79	0.012204
1.27	Flnc	cytoplasm, membrane	ankyrin binding	Complex	-1.27	0.042248
1.27	Psd2	membrane	ARF protein signaling	Complex	-1.15	0.036179
1.27				NonCoding	-1.29	0.049397
1.27				NonCoding	-1.44	0.023038
1.27	Gm4567			Coding	-1.34	0.025672
1.27				NonCoding	-2.74	0.026587
1.27	Gm13964			NonCoding	-3.13	0.041165
1.27	Gm19299			NonCoding	-1.43	0.04456
1.27				NonCoding	-1.58	0.046363
1.27				NonCoding	-1.48	0.047016
1.27	Gm15337			Complex	-1.66	0.047524
1.26	Speg	nucleus	ATP binding	Complex	-1.25	0.013933
1.26	Snx18	cytoplasmic vesicles	endocytosis and vesicle trafficking	Complex	-1.31	0.000159
1.26	Gm216			Coding	-1.38	0.016905
1.26	Abcc12	membrane	ATP binding	Coding	-1.14	0.016901
1.26	Lhcgr	cell membrane	hormone receptor activity	Complex	-1.47	0.016005

Appendix B (Continued)

1.26	Vmn2r-ps104			Complex	-1.39	0.004112
1.26				NonCoding	-1.43	0.004154
1.26	Bdh2	cytoplasm	NAD binding and oxidoreductase activity	Coding	-1.2	0.049147
1.26	1700013D24Rik			Coding	-1.69	0.007335
1.26	Abhd3	plasma membrane	phospholipase activity	Coding	-1.11	0.010033
1.26	Aldh111	cytoplasm	catalytic activity	Complex	-1.37	0.014017
1.26	Pled1	cytoplasm	calcium binding	Complex	-1.17	0.02152
1.26				NonCoding	1.09	0.015683
1.26	Ucp3	mitochondrion inner membrane	transporter activity	Complex	1.24	0.017429
1.26	RP24-282D16.2			NonCoding	-1.17	0.019562
1.26	Mir181a-1			NonCoding	-1.47	0.023429
1.26				NonCoding	-1.15	0.029822
1.26	Ltb	cell membrane	GPCR pathway	Complex	-1.39	0.030241
1.26	Lrrc46		regulation of protein stability	Coding	-1.17	0.034445
1.26	Gm973			Coding	1.25	0.03956
1.26	Gm14966			NonCoding	-2.1	0.046764
1.25	Esr1	nucleus	nuclear hormone receptor	Complex	-1.27	0.016041
1.25	Rlbp1	cytoplasm	retinol binding	Coding	1.27	0.000419
1.25	Vmn2r124	cell membrane	GPCR activity	Coding	-1.18	0.001197
1.25	Dnah6	cytoplasm	ATPase activity, ATP binding	Coding	-1.14	0.016468
1.25	Gm16833			Complex	-1.15	0.004009
1.25				NonCoding	-1.22	0.00439
1.25	Gm11027			Coding	1.23	0.004963
1.25	Gm14941			Complex	-1.29	0.046194
1.25	Cyp4f15		iron ion binding	Complex	-1.29	0.006485
1.25	Bpi	secreted, cytoplasmic granule membrane	immune response	Coding	-1.29	0.007546
1.25	Gm14089			NonCoding	1.74	0.007563
1.25	Hrsp12	cytoplasm, nucleus, peroxisome, mitochondrion	RNA binding	Complex	-1.26	0.01608
1.25	Ttc30a2	cilium	intracellular transport	Coding	-1.72	0.009072
1.25	Efcab12		calcium ion binding	Complex	-1.33	0.009211
1.25	Smyd1	cytoplasm and nucleus	DNA binding	Complex	1.48	0.033989
1.25	Myl2	cytoplasm	calcium ion binding	Complex	-1.25	0.024207
1.25				NonCoding	-1.46	0.013069
1.25	9130015L21Rik			NonCoding	-1.11	0.016206
1.25				NonCoding	-1.24	0.016815
1.25	P2ry10	cell membrane	GPCR activity, purinergic receptor activity	Coding	-1.27	0.017063
1.25	Gm3654			Pseudogene	-1.36	0.039165
1.25	Gm20482			Complex	1.89	0.033344
1.25	Gpre5d	cell membrane	GPCR activity	Coding	-1.16	0.023786
1.25	Ak9	cytoplasm and nucleus	ATP binding , catalytic activity	Complex	-1.3	0.028503
1.25	Ak312-ps			Pseudogene	1.05	0.030009
1.25	Fam198a	secreted		Coding	-1.13	0.030661
1.25	Ctdp1	nucleus and centrosomes	catalytic activity	Complex	-1.54	0.036714
1.25				NonCoding	-1.41	0.047184
1.25	Ucma	secreted	negative regulation of osteoblast differentiation	Complex	1.24	0.047387

Appendix B (Continued)